UNIVERSITY OF CALIFORNIA,
IRVINE

# Role of sulfidation in nanoscale zero-valent iron's arsenic immobilization and ecotoxicity in soil

THESIS

submitted in partial satisfaction of the requirements
for the degree of

MASTER OF SCIENCE

in Civil and Environmental Engineering

by

Ziwei Han

Thesis Committee:
Professor Adeyemi S. Adeleye, Chair
Professor Sunny Jiang
Professor Diego Rosso

2020

# TABLE OF CONTENTS

# LIST OF FIGURES

# LIST OF TABLES

# ACKNOWLEDGMENTS

First of all, I am grateful to Professor Adeyemi S. Adeleye for his guidance and the encouragement he gave me during my study. His supervision and suggestions helped me to complete the project. I also want to thank Professor Sunny Jiang and her student, Yen Hsiang Huang, for providing an ultra-low freezer for my lyophilized samples. I appreciate Praveen Krishna Veerasubramanian for his help with sample lyophilization.

Besides, I appreciate Yixin Zhao for working with me to explore the synthesis of nZVI and SnZVI. Although we were unfamiliar with nanoparticle synthesis when we started and failed several times, her encouragement helped me to not give up. In addition, I would like to thank members of the Adeleye Lab, Omobayo Salawu and Dr. Jenny Zenobio, for their help with BET and XRD analyses. I also acknowledge Chenglin Liu and Yixin Zhao for their assistance with earthworm upkeep.

Finally, I want to say thank you to my parents, friends, and lab colleagues for their great help and encouragement.

# ABSTRACT OF THE THESIS

Role of sulfidation in nanoscale zero-valent iron's arsenic immobilization and ecotoxicity in soil

by

Ziwei Han

Master of Science in Civil and Environmental Engineering

University of California, Irvine, 2020

Professor Adeyemi S. Adeleye, Chair

Arsenic (As) is widely distributed in soil in the United States and around the world, highly toxic, and not efficiently remediated by existing traditional methods. Nanoscale zero-valent iron (nZVI)-based remediation is an emerging technology that has successfully been used to immobilize metals and metalloids due to nZVI's high surface area and strong reducing ability. However, immobilization efficiency of nZVI decreases over time due to its oxidation under natural conditions. Modification of nZVI via sulfidation, to produce sulfide-modified nZVI (SnZVI), has been shown to overcome some of the shortcomings of nZVI. The main objective of this study was to compare the immobilization performance of nZVI and SnZVI for As in soil and determine if the toxicity of nZVI is influenced by sulfidation. The immobilization efficiency of nZVI and SnZVI (0.3, 1, and 5 wt.%) for As (50 ppm) in soil was monitored for 112 days under aerobic and anoxic conditions. The aerated soil also contained earthworms (*Eisenia fetida*) to evaluate the toxic impacts of the nanoparticles-based remediation. In general, SnZVI had a slower reaction kinetics, leading to lower As immobilization efficiency than nZVI after 7 days at 0.3 and 1% group. However, after 112 days,

sulfidation was found to inhibit the corrosion of nanoparticle under aerobic conditions and the immobilization efficiency was similar to that of nZVI at all nanoparticle dosage concentrations. Both nanoparticles were toxic to *E. fetida*, but SnZVI was remarkably less toxic than nZVI. This study demonstrates the potential of SnZVI for effective and sustainable remediation.

## 1. Introduction

Arsenic (As) is a metalloid that is widely distributed in the natural environment, such as in dust [1], groundwater [2,3], and soil [4]. In certain regions, high concentrations of As can be naturally introduced into the environment due to the geological formations [5]. Also, anthropogenic activities such as batteries production [6] and mining [7] are potential sources of As pollution. Similarly, feeds [8], pesticides [9], and herbicides [10] used in agriculture can cause massive amounts of As to enter the environment. According to a 2017 report by the United States Geological Survey (USGS), 10% of all surface soil (0-5 cm) in the United States (US) has 10 – 166 ppm of As contamination (Figure 1) [11]. As in soil can accumulate in the food chain, leading to human exposures [12,13]. As is highly toxic to humans, due to its carcinogenic, bioaccumulative, [14] and biomagnification [15] properties. Studies have shown that human exposure to 0.6 mg/kg/day inorganic As can cause acute lethality [16]. To indicate the gravity of As contamination in the US, As topped the 2019 priority list of hazardous substances jointly published by the Agency for Toxic Substance and Disease Registry (ATSDR) and the US Environmental Protection Agency (EPA)[17].

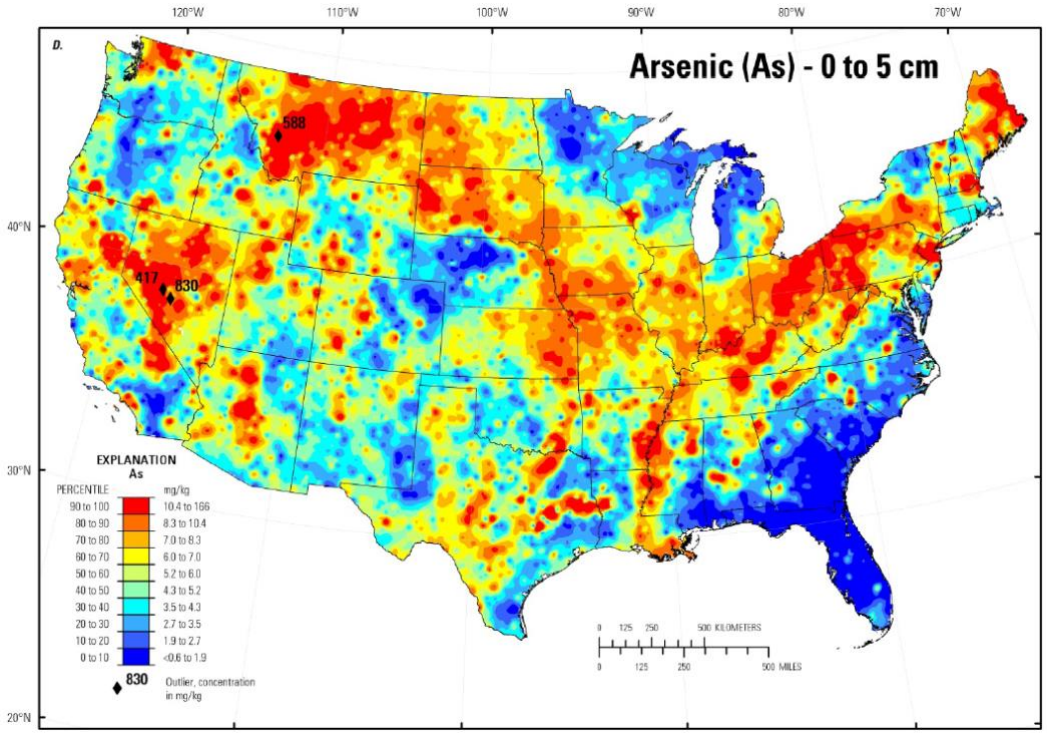


Figure 1. The concentration of As in the surface soil (0 – 5 cm) in the United States. Source: United States Geological Survey [11]

For unrestricted use soil, the US EPA recommends that As should not exceed 0.39 mg/kg (390 ppb) [18]. The methods currently used to decrease bioavailable inorganic As in soil include bioremediation [19,20], soil acid-wash [21], and adsorption/co-precipitation with particles [22]. Soil acid-wash is simple but entails consumption of a large amount of acids and bases. More so, the method is not environment-friendly because acids and bases are toxic to organisms and may leach out beneficial ions from soil. Bioremediation of soil As is commonly performed using microorganisms and plants. *Pseudomonas putida* KT2440, a soil bacterium, can induce the conversion of inorganic As into less toxic organic As [19]. Similarly, plants such as vetiver grasses, can adsorb As by releasing organic matter from their roots, or co-precipitate As by producing organic sulfides [20]. The main disadvantage of bioremediation techniques is that it is not applicable to all

soil types, and it takes a long time. Materials, such as biochar [23], as well as some iron-containing particles (such as zero-valent iron [24] and goethite [25]), can efficiently immobilize As in the soil through adsorption and/or co-precipitation.

Nanotechnology methods, based on the use of nanoscale zero-valent iron (nZVI), are an emerging and viable option for *in situ* remediation of organic and inorganic pollutants, as demonstrated by several bench, pilot, and field studies [26–29]. nZVI immobilizes heavy metals and metalloids due to its high surface area and strong reducing ability (standard reduction potential [$E°$] = -440 mV) [30,27,31]. In water, nZVI has been effectively used to remove metals including copper (Cu) [32], cadmium (Cd) [33,34,35], chromium (Cr) [36], lead (Pb) [37], Zinc (Zn) [37], and As [32]. In the natural environment, As is mostly present as arsenite As(V) and arsenate As(V) [38]. Arsenic Speciation in Environmental Samples of Contaminated Soil. Previous studies have shown that As(V) is mainly adsorbed by nZVI. In addition, some As(V) may be reduced to As(III) or $As_0$, both of which are then be adsorbed or co-precipitated with iron oxide on the surface of nZVI [32,30] (Figure 2).

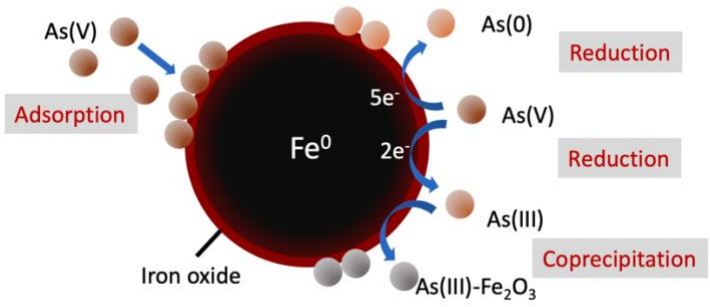


Figure 2. The mechanisms of As immobilization by nZVI

However, the high reduction activity of nZVI makes it extremely susceptible to oxidation in the natural environment. More so, nZVI undergoes a side reaction with water (Eq. 1), which consumes the nanoparticles. Both of these reactions lead to the transformation of nZVI, which weakens its long term metal immobilization efficiency [39]. Additionally, nZVI is toxic to organisms due to increase in iron ( $Fe^{2+}/Fe^{3+}$) concentrations in the environment [40]. Reactions of nZVI and its byproducts may also lead to production of reactive oxygen species (ROS), which induces oxidative stress on biological cells [41]. nZVI particles are magnetic; hence, they agglomerate to micronscale sizes rapidly [42]. The large size of the nZVI agglomerates limits their mobility, and thus application of nZVI for groundwater remediation [43]. These weaknesses have slowed down the adoption of nZVI for pollution contamination in natural waters and soils.

$$Fe^0(s) + 2H_2O(aq) \rightarrow Fe^{2+}(aq) + H_2(g) + 2OH^-(aq) \quad (1)$$

To improve the performance of nZVI, it has been modified by co-doping with metals to produce bimetallic nanoparticles, immobilization on activated carbon and other materials to decrease agglomeration, and sulfidation to produce sulfide-modified nZVI (SnZVI) [43]. In particular, SnZVI possesses improved reactivity (relative to nZVI) for some pollutants [44], better colloidal and chemical stability [43,33], and superior electron transfer potential [36]. Also, the FeS formed in SnZVI is an excellent co-precipitating agent for several metals and metalloids, including As [45,46]. In addition, SnZVI is more hydrophobic than nZVI, decreasing the tendency to undergo side reactions with water [47]. Studies have demonstrated that SnZVI has a higher immobilization efficiency than nZVI for Cd [33,34,35] and Cr [36] in aqueous solution. However, there is no study on the applicability of SnZVI for remediating As-contaminated water or soils. In addition, most laboratory studies on contaminant remediation do not consider the concomitant effect of the remediation

strategy on the ecosystem. This study was performed to test the hypothesize that SnZVI will perform better than nZVI in immobilizing As in soil due to SnZVI's lower affinity for water, and SnZVI will exhibit lower toxicity to soil organisms than nZVI due to the higher chemical stability of SnZVI.

In this thesis, nZVI was synthesized and modified via sulfidation to prepare SnZVI. Both nZVI and SnZVI were then applied for the remediation of As-contaminated soil in the presence of earthworms (*Eisenia fetida*). The applicability and implications of both nanotechnology-based methods for soil remediation were thereafter evaluated. The main objectives of this thesis were to (1) compare the long-term immobilization performance of nZVI and SnZVI for As(V) in soil; (2) determine if nanoremediation alleviated or exacerbated the toxic impact of As to a soil organism, *E. fetida*; and (3) explore the mechanism of As immobilization by the nanoparticles in order to optimize the technology for future field implementation.

## 2. Materials and Methods

### 2.1. Nanoparticles synthesis and characterization

Both nZVI and SnZVI were synthesized under nitrogen atmosphere using previously published methods and solutions were prepared with deoxygenated deionized (DI) water (18.2 MΩ.cm, Milli-Q Ultrapure Water Systems) [47]. Briefly, to prepare nZVI and SnZVI, 270 mL of 1 M sodium borohydride ($NaBH_4$; Acros Organics, Morris Plains, NJ) was mixed with 30 mL of 0 M and 0.021 M sodium dithionite ($Na_2S_2O_4$; Millipore Sigma, Burlington, MA), respectively; and then titrated into 300 mL of 0.15 M ferric chloride ($FeCl_3$; Alfa Aesar, Ward Hill, MA) at a flow rate of 10 mL/min to achieve a theoretical sulfur/iron (S/Fe) molar ratios of 0 (nZVI) or 0.28 (SnZVI). The mixture was continuously stirred at 600 rpm for 15 min. The nanoparticles were then separated from aqueous media using a Neodymium magnet and washed with deoxygenated DI water three times. Finally, the nanoparticles were dried using a vacuum oven (Napco, Model 5831, Scotia, NY), ground with a mortar, and stored under vacuum till use.

A Magellan 400 scanning electron microscope (SEM, FEI, USA) was used to determine the size and morphology of the nanoparticles. The phase and crystal structure of nanoparticles were determined using an Ultima-III X-ray diffractometer (XRD; Rigaku, Japan). The Brunauer-Emmett-Teller (BET) surface area was determined using a Micromeritics 3Flex Surface Characterization Analyzer (Norcross, GA). Hydrodynamic size and zeta ($\zeta$) potential of both nanoparticles were determined using a NanoBrook 90Plus (Brookhaven Instruments, Holtsville, NY), employing established methods [48].

## 2.2. Soil preparation and characterization

Artificial soil was used for this study to reduce the confounding interactions of various components present in natural soils. The soil was prepared according to OECD 207 guideline [49] The soil was composed of 69% sand (Quikrete, Atlanta, GA), 10% peat moss (Miracle-Gro, Marysville, OH), 20% kaolin clay (Bulk Apothecary, Aurora, OH), and 1% calcium carbonate ($CaCO_3$, Fisher Scientific, Hampton, NH) for pH adjustment. Moisture was maintained at 50-60% of the soil water holding capacity (WHC, which was determined following the method prescribed by OECD 207). The organic matter content of the soil was assessed according to the Loss-on-Ignition (LOI) method [50]. In addition, the BET surface area of soil was determined using the Micromeritics 3Flex Surface Characterization Analyzer and the major

## 2.3. Adsorption isotherm study

According to the literature, one of the main mechanisms of As removal by nZVI is adsorption. In soil pore water, competitive adsorption for As will occur between soil and nZVI/SnZVI. Hence, adsorption isotherm experiments were performed in aqueous media to compare the affinity and capacity for As between the two nanoparticles and soil. For the adsorption study, 20 mL of solution containing 500 mg/L of the solid phase (that is, nZVI, SnZVI or soil) and 20, 40, 60, 80, 100 mg/L of As (from $Na_2HAsO_4$, Alfa Aesar) were shaken at 150 rpm and 20 ℃ for 150 min using a Versa-Bath S Model 224 (Fisher Scientific, Hampton, NH). Each treatment was set up in triplicates. At the end of 150 min, each mixture was passed through a 0.22 μm PVDF filter (ChromPure, Auburn, WA) and the concentration of As and Fe in the filtrate was measured via inductively coupled plasma mass spectrometry (ICP-MS) using a Thermo iCAPRQ-C2 ICP-MS (Waltham, MA). The ICP-MS was calibrated with a NIST-traceable standard obtained from Thermo

Scientific. The experimental results from the adsorption studies were analyzed using the following four adsorption isotherm models:

### 2.3.1. Langmuir Isotherm

Langmuir Isotherm is a monolayer adsorption model. As such, saturation is reached after adsorbates (As) fills the surface of the adsorbent. The maximum adsorption capacity can be obtained at saturation point/time. The linear form of the Langmuir model is shown in Eq. 2.

$$\frac{1}{q_e} = \frac{1}{q_m} + \frac{1}{K_L q_m}\frac{1}{C_e} \quad (2)$$

where $q_e$ and $C_e$ are the adsorption capacity (mg/g) and concentration (mg/L) at equilibrium state. $K_L$ is Langmuir constant, which is related to adsorption energy, and $q_m$ is the maximum adsorption capacity (mg/g). The parameter, $q_e$, is defined according to Eq. 3.

$$q_e = \frac{amount\ of\ adsorbate\ adsorbed\ at\ equilibrium\ state,\ \ mg}{amount\ of\ adsorbent\ used,\ \ g} \quad (3)$$

Also, a converted Langmuir isotherm (Eq. 4) is also commonly used to fit adsorption isotherm data.

$$\frac{C_e}{q_e} = \frac{1}{q_m} C_e + \frac{1}{K_L q_m} \quad (4)$$

### 2.3.2. Freundlich Isotherm

The Freundlich Isotherm assumes that the adsorbates could be adsorbed on heterogeneous surfaces, which is suitable for monolayer and multi-layer adsorption. The linear form of the equation is shown in Eq. 5:

$$log\ q_e = log\ K_F + \frac{1}{n} log\ C_e \quad (5)$$

where $K_F$ is Freundlich constant, which is related to adsorption capacity, and n is an empirical value, which

is related to adsorption intensity.

2.3.3. Temkin Isotherm

The Temkin isotherm describes the linearly decreasing adsorption energy as the adsorbates cover the surface of the adsorbent. The linear form of the equation is shown in Eq. 6.

$$q_e = \frac{RT}{b} ln\, K_T + \frac{RT}{b} ln\, C_e \quad (6)$$

where $K_T$ is the Temkin constant (L/g), b is related to the heat of adsorption (J/mol), T is the temperature (K) and R is the gas constant (8.314 J/mol·K).

2.3.4. Dubinin-Radushkevich (D-R) Isotherm

The D-R isotherm assumes the pore filling mechanism for adsorption, and is typically applied for physical adsorption. The linear form of model is shown in Eq. 7:

$$\ln q_e = \ln q_d - \beta\varepsilon^2 \quad (7)$$

where $q_d$ is the D-R constant (mg/g), β is related to free energy, and ε is the Polanyi potential. The Polanyi potential is defined by Eq. 8:

$$\varepsilon = RT\ ln\ (1 + \frac{1}{C_e}) \quad (8)$$

**2.4. Soil remediation with nanoparticles**

2.4.1. As immobilization

To test the hypothesis that sulfidation will increase the immobilization efficiency of nZVI for As in soil, we performed As immobilization studies in soil under aerobic and anoxic conditions. Soil was spiked with

$Na_2HAsO_4$ stock solution to achieve a final concentration of 50 mg As/kg soil (ppm). This concentration falls in the range of soil As concentration in many places, including the US [51–53]. The contaminated soil was allowed to equilibrate for one day, after which nZVI and SnZVI were mixed into the As spiked soil to achieve 0, 0.3, 1 and 5% (*w*/*w*; nanoparticle/soil). These nanoparticle concentrations were decided based on the effective concentrations reported by previous nZVI-based remediation bench and field studies [29,52]. The treated soils were placed in a temperature-controlled room (20 ± 2°C) under 16-8 h light-dark cycle. Each treatment was setup in triplicates. A fraction of the soil was analyzed for leachable As on days 0 (immediately after adding As), 7, 28, 56, and 112 after lyophilization (Labconco Freeezone 4.5, Kansas, MO). Leachable As was measured according to a previous study [54]. Briefly, 2 g of lyophilized soil was mixed (150 rpm; Versa-Bath S Model 224 ) with 15 mL DI water at 20°C for 2 h and then centrifuged (3000 *g*, 15 min) using a Beckman J2-21 M/E (Indianapolis, IN). The supernatant was filtered (ChromPure 0.22 μm PVDF filter) and diluted before As analysis using the iCAPRQ-C2 ICP-MS. The immobilization efficiency of each nanoparticle was determined using Eq. 9:

$$As\ immobilization\ efficiency\ (\%) = \left(\frac{Final\ concentration\ of\ leachable\ As}{Initial\ concentration\ of\ Leachable\ As\ on\ day\ 0}\right) \times 100\% \quad (9)$$

2.4.2. Modeling of As immobilization with artificial neural network (ANN)

Although there are several adsorption studies, most of them were conducted in aqueous media and are related to kinetics or isotherms. Adsorption models, such as Langmuir isotherm or Freundlich isotherm, are helpful for gaining a deeper understanding of the mechanism of adsorption. However, in practical applications, the dosage of adsorbents (nanoparticles) is one of the most important parameters. Since there is no models for estimate the nanoparticle dosage needed to achieve a given contaminant immobilization,

this study relied on the emerging neural network technology to initially establish, evaluate and predict the performance of different nanoparticle dosages for future applications.

In this study, four sets of immobilization efficiency data (the two nanoparticles (nZVI/SnZVI) at two timepoints, day 7 and 28) were individually input into MATLAB_R2018b Neural Net Fitting application. Each set of data was only used for predicting the result for one nanoparticle at one timepoint. Respectively, 50%, 25%, and 25% of data was used for training, validation, and testing sections for machine learning. The Levenberg-Marquardt algorithm with two hidden layers was used for training. The output functions were accepted when the correlation coefficients of target and output were higher than 0.95 in training, validation, and testing.

2.4.3. Mechanism of remediation via X-ray diffraction analysis

To explore the mechanism of As remediation by nZVI and SnZVI, another batch of soil remediation study was set up under aerobic and anoxic conditions. In this study, however, the concentrations of nanoparticles and As were increased to 30% and 50 g As/kg-soil, respectively, to obtain sufficient signal for XRD analysis. The nanoparticle-treated As-contaminated soils were then placed in a temperature-controlled room (20 ± 2°C) under 16-8 h light-dark cycle for 7 d before XRD analysis. Aliquots of the treated soils were lyophilized to stop the reactions, and then analyzed using the Ultima-III X-ray diffractometer after lyophilization the samples.

## 2.5. Environmental impact of nanoremediation

### 2.5.1. Effect on soil pH

Several soil organisms are sensitive to pH changes and can only survive within a narrow pH range [55]. To understand how nZVI/SnZVI-based nanoremediation may influence the survival of pH-sensitive species, additional experiments were set up similar to the immobilization efficiency study. As-contaminated soils were treated with nZVI or SnZVI (0.3, 1, and 5%). Control treatment consisted of the same amount of soil but without As and nanoparticles. Soil pH was measured over time according to ISO-10390 method [56]. In brief, about 5 g of soil was dried at room temperature for 12 h, and then mixed with 10 mL of 0.01 M $CaCl_2$ (Alfa Aesar) for 5 min using the Versa-Bath S Model 224. The mixture was allowed to stabilize for 2 h, after which the pH of the supernatant was measured using an Accumet AB200 pH meter (Fisher Scientific).

### 2.5.2. Effect on soil organism

To quantify the toxicity of As in soil environments, the survival of *E. fetida* (The Worm Farm, Durham, CA) in soil spiked with 0, 10, 40, 80, 150, and 300 ppm As was determined in a two-week study performed according to OECD guideline 207 [49]. The experimental data was used to determine the $LC_{50}$ of As to *E. fetida*, using logistic model shown in Eq. 10:

$$Mortality(\%) = \frac{L}{1+e^{-k(t-t_0)}} \quad (10)$$

where t is the time (week); $t_0$ is the t value at the sigmoid plot's midpoint; L is the maximum mortality; and k is the logistic growth rate.

To test the hypothesis that sulfidation will decrease the toxicity of nZVI in soil environments, additional

tests were performed in the presence of As only (50 ppm), nanoparticles only (0.3% and 1% nZVI or SnZVI), and combinations of As and nanoparticles. Preliminary studies showed that the highest concentration of nanoparticles used for immobilization (5%) was extremely toxic and it was not used for this study. For each treatment, 10 adult earthworms (300-600 mg each, with clitellum) were introduced into the As-contaminated soil (500 g), with or without 0.3 and 1% of nanoparticles. Control treatments contained neither As nor nanoparticles. The experiment was carried out in triplicates at 20 ± 2°C under 16/8 h light-dark cycles. The soil WHC was maintained at 50 - 60% throughout the study. The survival (calculated using Eq. 11) of earthworms was determined every 7 d for 28 d (as recommended by the OECD guideline). The average weight of live earthworms in each treatment was measured at the end of the toxicity study (day 28).

$$Survival\ (\%) = \frac{Number\ of\ live\ earthworms}{Initial\ number\ of\ earthworms} \times 100\% \quad (11)$$

2.5.3. Effect of pH on earthworm survival

We observed substantial increase in soil pH during the toxicity tests performed in the presence of nZVI and SnZVI. To determine if the pH increase explains some of this toxicity observed in the presence of the nanoparticles, pH-control toxicity tests were performed in the absence of As and nanoparticles. Like the toxicity experiments, 10 adult earthworms (300-600 mg each, with clitellum) were introduced into the 500 g of uncontaminated soil with pH 6, 7, 8, and 9. The survival of earthworms was determined every 7 d for 28 d, and the average weight of live earthworms was measured on day 28.

## 2.6. As bioaccumulation by *E. fetida*

In addition to the toxicity endpoint prescribed by OECD 207 (that is, survival), As bioaccumulation by *E.*

*fetida*, kept in As contaminated soil with and without nZVI/SnZVI for 28 d, was determined at the end of the toxicity experiments. Only live worms were used for metal bioaccumulation assays. The earthworms were placed on moist filter paper for 24 h to void their gut contents. To measure tissue As content, 0.1 g of dried, pulverized earthworm was digested with 2 mL of trace-metal grade $HNO_3$ (Fisher Scientific), using a temperature sequence of 80 ℃ for 2 h, and then 135 ℃ for 1 h [57]. The digestate was cooled down, passed through a 0.22 μm PVDF filter, diluted with DI water, and analyzed via ICP-MS. Bioaccumulation factor (BAF) for the worms was calculated using Eq. 12.

$$BAF = \frac{Concentration\ of\ As\ in\ earthworms}{Concentration\ of\ As\ in\ soil} \quad (12)$$

### 2.7. Data and statistical analysis

Experimental data were tested for normality using the Shapiro-Wilk method and significance using two-way Analysis of Variance (ANOVA) followed by two-sample Tukey's test (SPSS Statistics version 25.0). Normality was accepted when $p > 0.05$. A statistically significant difference for ANOVA and post hoc tests was defined as $p \leq 0.05$.

## 3. Results and Discussions

### 3.1. Nanoparticles characterization

The major characterization of nZVI and SnZVI were summarized in Table 1. Both nZVI and SnZVI were negatively charged at pH 7, based on the zeta (ζ) potential values of -25.05 mV (for nZVI) and -15.81 mV (for SnZVI) determined via electrophoretic light scattering analysis. These ζ potential values are well below the threshold of colloidal stability (± 30 mV) [58], suggesting that the nanoparticles would agglomerate at pH 7. The hydrodynamic diameter, measured via dynamic light scattering method, showed that the agglomerates formed by nZVI (280.6 nm) are slightly smaller than those formed by SnZVI (286.5 nm).

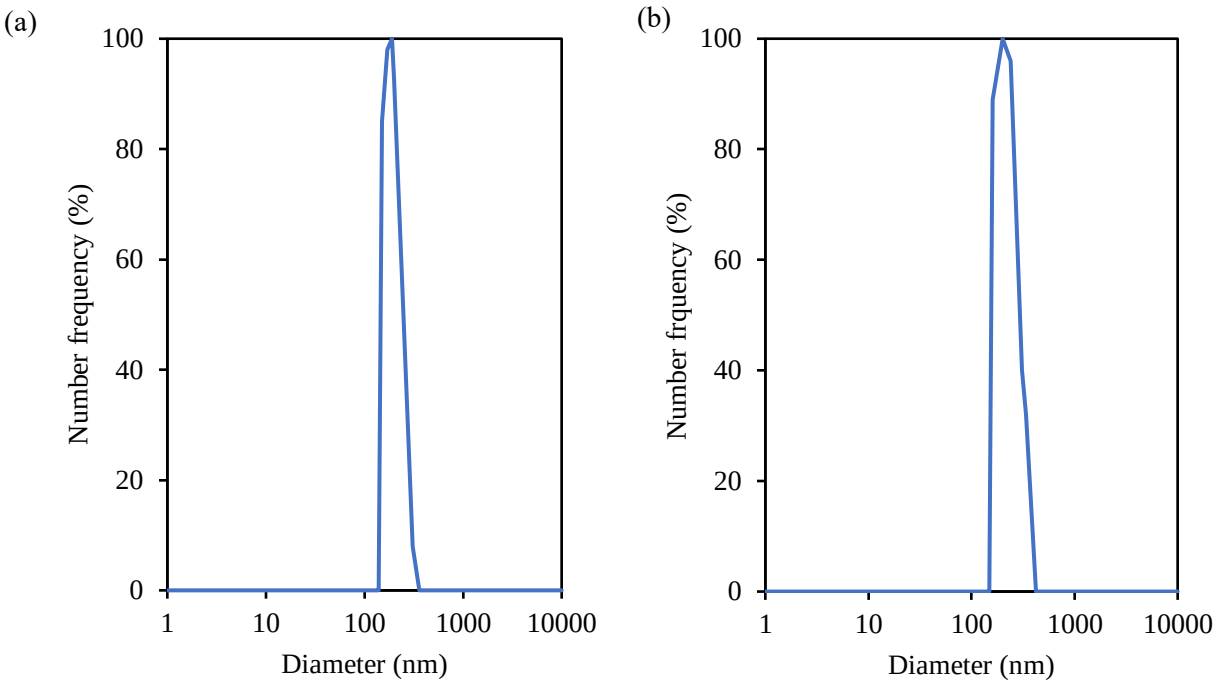


Figure 3. The number-based hydrodynamic size distribution of (a) nZVI and (b) SnZVI in water at pH 7

The XRD diffractograms of nZVI and SnZVI are shown in Figure 4. The characteristics peaks of zerovalent

iron ($Fe_0$) at 2θ = 45° and 83° were observed in the freshly synthesized nZVI and SnZVI. In addition to $Fe_0$, other chemical phases of Fe were observed in both nanoparticles, namely, $Fe_3O_4$ (at 2θ = 31° and 48°) and FeS (at 2θ = 65°), observed in nZVI and SnZVI, respectively. The presence of $Fe_3O_4$ in nZVI is common, due to the core-shell structure of the nanoparticle, with the iron oxide shell surrounding the core of $Fe_0$. The XRD data confirms the expected chemical composition of both nanoparticles, and shows that SnZVI is less prone (than nZVI) to oxidation in ambient conditions.

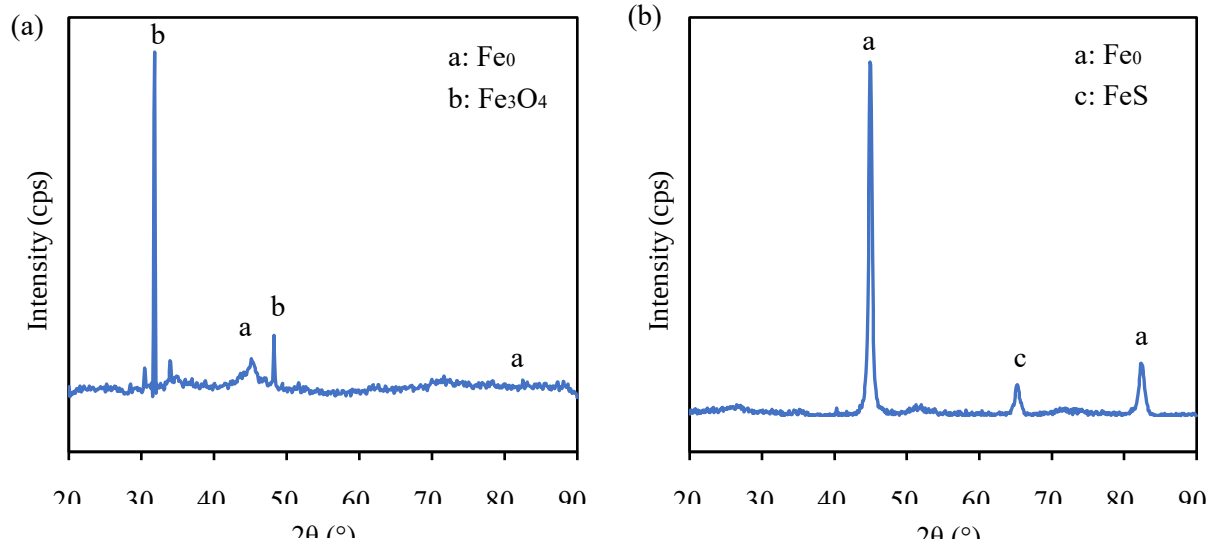

Figure 4. XRD diffractograms of (a) nZVI and (b) SnZVI

The mean specific surface area of nZVI (118.77 $m_2/g$) was much higher than that of SnZVI (41.39 $m_2/g$). Additionally, the average pore size of nZVI and SnZVI were measured to be 9.02 and 9.75 nm, respectively; while the total pore volume of nZVI and SnZVI were 0.56 and 0.22 $cm_3/g$, respectively (Table 1). Sulfidation decreases the formation of oxides on the surface of nZVI, resulting in less pore volume. The drastic decrease in surface area upon sulfidation is likely due to increase in crystal/particle size as shown

by the peak size of the $Fe^0$ phase in the XRD data. The lower surface area of SnZVI may result in decreased adsorption capacity and immobilization efficiency, compared to nZVI.

Table 1. Major physicochemical properties of the nanoparticles used in this study

| **Parameters** | **Nanoparticles** | |
|---|---|---|
| | **nZVI** | **SnZVI** |
| Hydrodynamic diameter (nm) | 280.62±9.21 | 286.53±2.84 |
| ζ potential (pH = 7, mV) | -25.05±8.49 | -15.51±9.30 |
| BET surface area ($m^2/g$) | 118.77 | 41.39 |
| Crystal phases | $Fe^0$ and $Fe_3O_4$ | $Fe^0$ and FeS |
| Pore size (nm) | 9.02 | 9.75 |
| Pore volume ($cm^3/g$) | 0.56 | 0.22 |

### 3.2. Soil characterization

The major properties of the soil used in this study are summarized in Table 2. The WHC, pH, and organic carbon values were within the range recommended in OECD 207 and other similar publications [52]. Leachable As was not detected in the soil, which shows that the only source of As to the soil was through spiking. The surface area of the soil (5.30 $m^2/g$) was much less than those of the nanoparticles (Table 1). Additionally, the pore size and pore volume of soil was measured to be 1.25 nm and 0.002 $cm^3/g$, respectively.

Table 2. Properties of the OECD artificial soil used in this study

| Parameters | Value |
|---|---|
| WHC (%) | 17.94±1.29 |
| Organic carbon (%) | 2.45±0.24 |
| pH | 7.07±0.03 |
| Leachable As (ppm) | nd |
| BET surface area ($m^2/g$) | 5.30 |
| Pore size (nm) | 1.25 |
| Pore volume ($cm^3/g$) | 0.002 |

nd = not detected

### 3.3. Adsorption isotherm studies

#### 3.3.1. Langmuir isotherm

The Langmuir isotherm describes monolayer adsorption of adsorbates to adsorbents. In Eq. 2, $q_m$ reflects the maximum adsorption capacity of the adsorbent, while $K_L$ and $q_m$ are used to predict if adsorption is favorable, by calculating the separation factor, $R_L$, as shown in Eq. 13 [59]:

$$R_L = \frac{1}{1+K_L q_m} \quad (13)$$

Adsorption is considered favorable when $0 < R_L < 1$, linear if $R_L = 1$, irreversible when $R_L = 0$, and unfavorable when $R_L > 1$.

Based on the regression coefficient values shown in Figure 5, the adsorption of As onto soil is better described by the regular Langmuir model ($R_2$ = 0.9427) than the converted Langmuir model ($R_2$ = 0.1854). However, the values obtained for $q_m$ and $K_L$, after fitting the experimental data of As adsorption to soil, were for negative. This indicates that the Langmuir isotherm model was not suitable for describing the adsorption of As to soil. For the two nanoparticles, the regression coefficient values suggested that both Langmuir model and the converted Langmuir model were more suitable for describing the adsorption of As to SnZVI ($R_2$ = 0.9624 and 0.9977, respectively) than nZVI ($R_2$ = 0.8881 and 0.9470, respectively). Additionally, based on $R_L$ calculations (Table 3), the adsorption of As was favorable for both nZVI ($R_L$ = 0.26) and SnZVI ($R_L$ = 0.22). On a mass basis, the adsorption capacity estimated from the Langmuir model and the converted Langmuir model was higher in nZVI (31.25 and 37.31 mg/g, respectively) than in SnZVI (19.16 and 19.53 mg/g, respectively). This agrees with the possession of a higher surface area per unit mass by nZVI (118.77 $m_2$/g) than SnZVI (41.49 $m_2$/g). However, an estimation of surface area-normalized adsorption capacity ($q_N$, calculated using Eq. 143) showed a higher surface reactivity for SnZVI (0.46 and 0.47 mg/$m_2$, respectively) than nZVI (0.26 and 0.31 mg/$m_2$).

$$q_N(mg/m^2) = \frac{Adsorption\ capacity\ (mg/g)}{Surface\ area\ (m^2/g)} \quad (14)$$

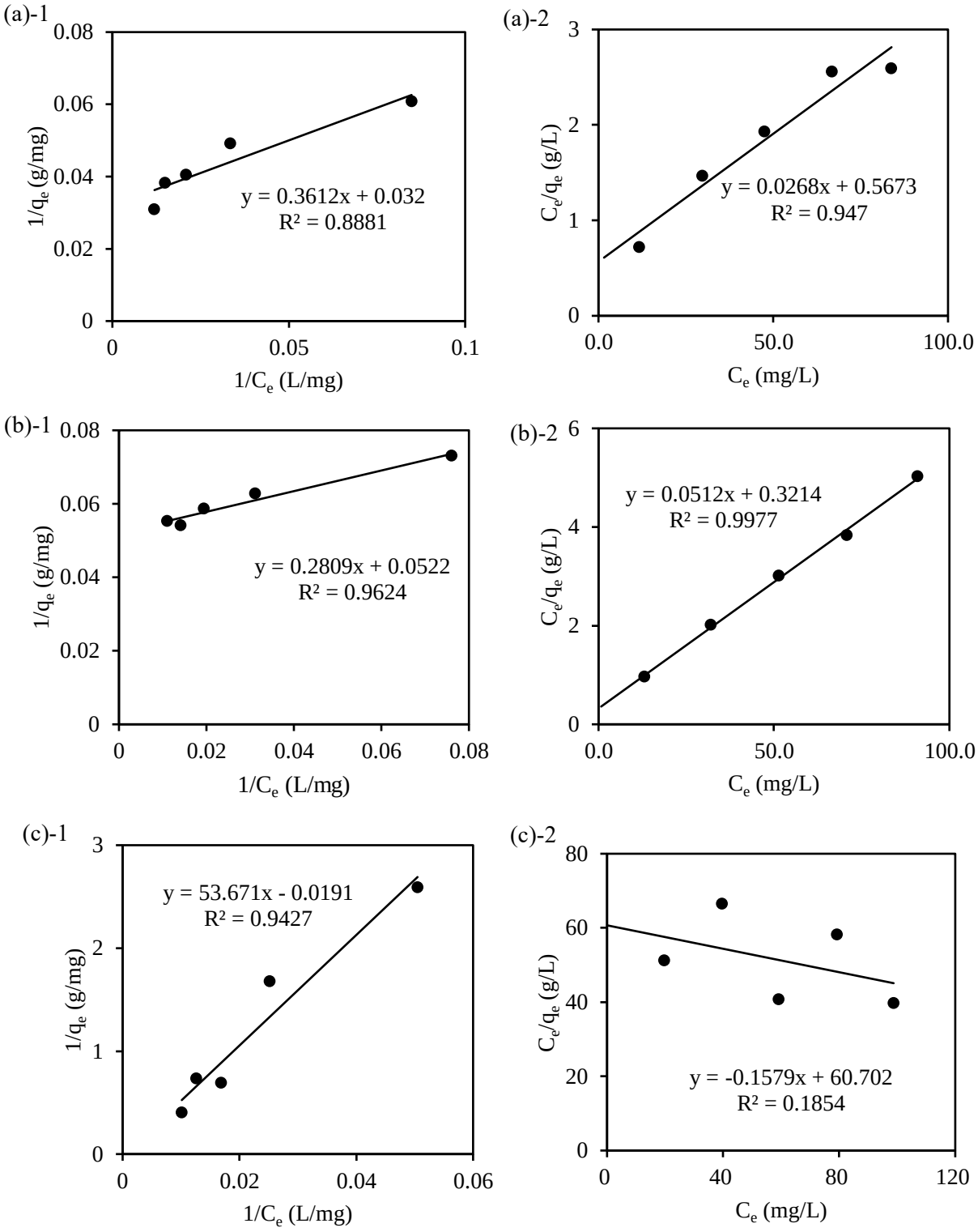


Figure 5. Modeling of adsorption of As to (a) nZVI, (b) SnZVI, and (c) soil (c) using (1) Langmuir isotherm and (2) converted Langmuir isotherm.

### 3.3.2. Freundlich isotherm

As shown in Figure 6, the regression coefficients obtained from fitting the As adsorption data obtained for the three solid phases with the Freundlich model suggests the model is generally suitable ($R^2$ > 0.9). The Freundlich isotherm is an empirical model for a heterogeneous surface. The parameter $\frac{1}{n}$ the Freundlich model (Eq. 4) is commonly used to evaluate adsorption intensity. Adsorption is favorable when $\frac{1}{n}$ < 1 and unfavorable when $\frac{1}{n}$ > 1. When $\frac{1}{n}$ = 1, the distribution between the two phases is independent of concentration [59]. The $\frac{1}{n}$ values obtained for nZVI (0.3221) and SnZVI (0.1556) indicated favorable adsorption of As by the two nanoparticles. The parameter suggests that the adsorption of As by soil is however unfavorable ($\frac{1}{n}$ = 1.1314). Moreover, based on the values of $K_F$, the trend of adsorption capacity for the solid phases were SnZVI (9.24) > nZVI (7.16) >>> soil (0.012).

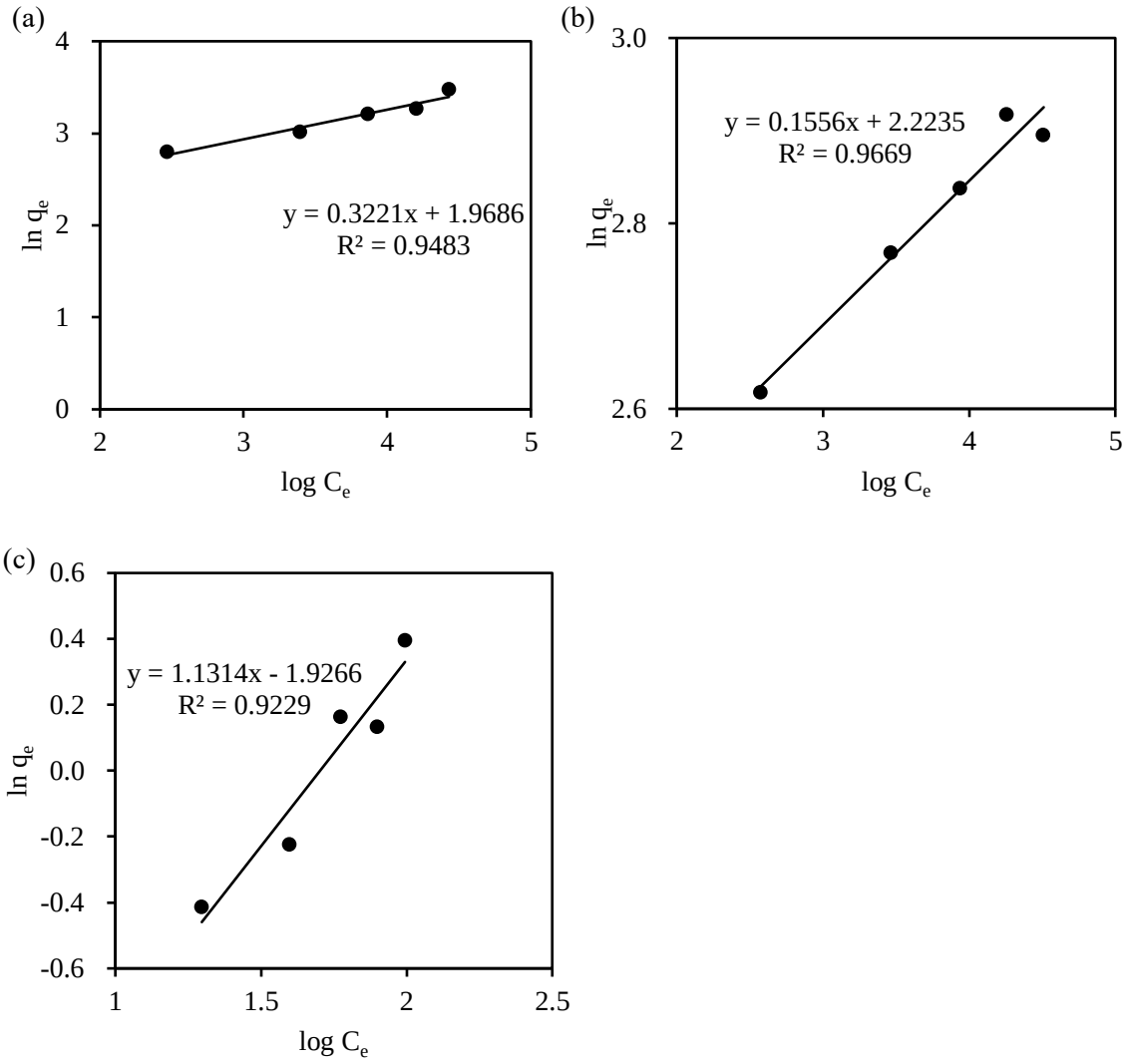


Figure 6. Modeling of adsorption of As to (a) nZVI, (b) SnZVI, and (c) soil (c) using Freundlich model

3.3.3. Temkin isotherm

The Temkin isotherm is an energy-related model for heterogeneous surfaces. According to the fitting model (Figure 7), SnZVI had a higher regression coefficient ($R_2$ = 0.9640) than nZVI ($R_2$ = 0.8936) and soil ($R_2$ = 0.7937). The parameter, b, reflects the thermal effect of the adsorption process. The reaction is endothermic when b > 0 and exothermic if b < 0 [60]. The reaction energy obtained for nZVI (b = 20.291 kJ/mol), was higher than that of SnZVI (b = 6.371 kJ/mol) and soil (b = 3.638 kJ/mol); but the adsorption

of As was endothermic for all the solid phases. This suggests that increase in temperature could increase the adsorption capacity of nZVI, SnZVI, and soil for As.

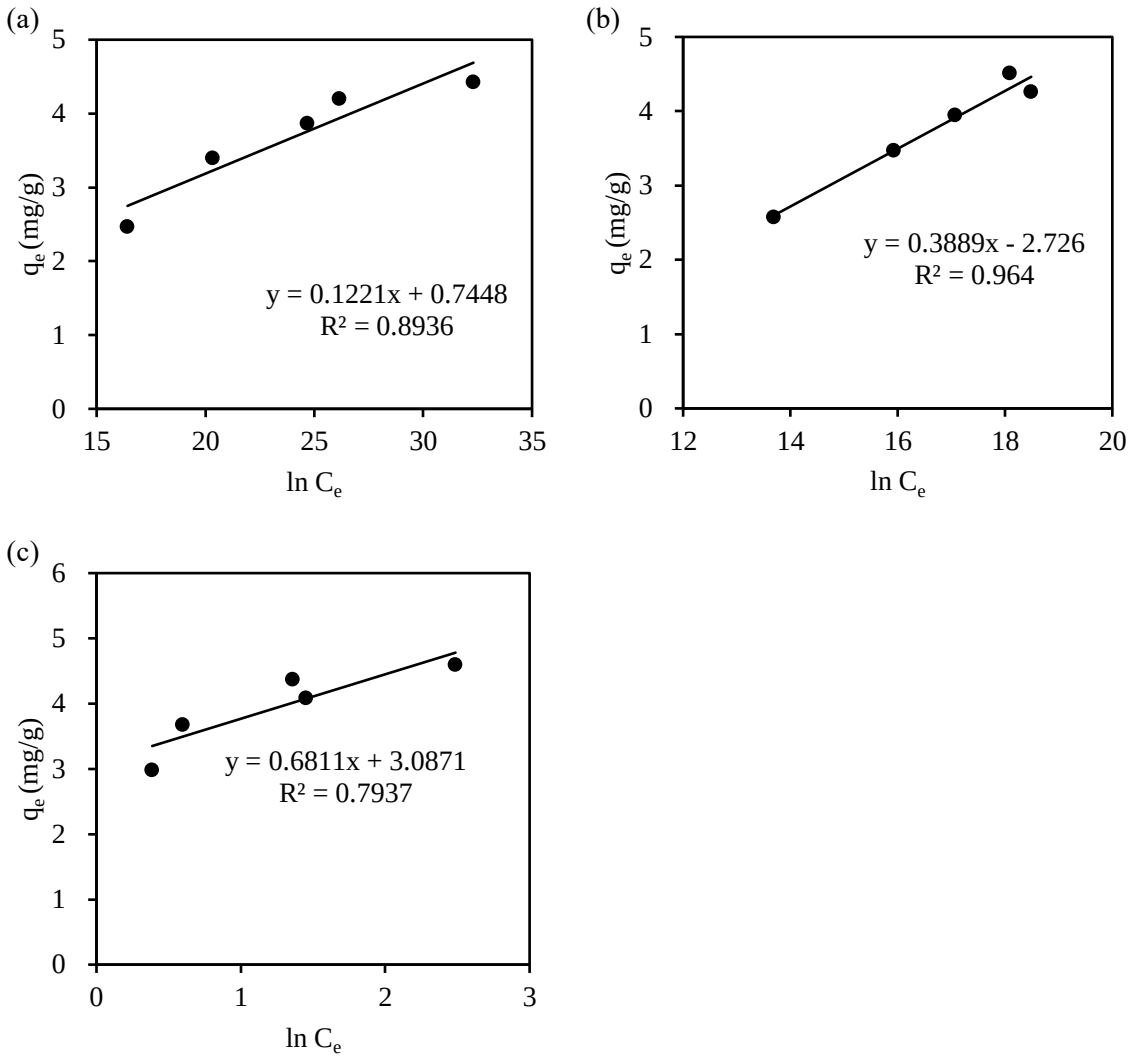


Figure 7. Modeling of adsorption of As to (a) nZVI, (b) SnZVI, and (c) soil (c) using the Temkin isotherm

3.3.4. D-R isotherm

The D-R isotherm is a model used to express the Gaussian energy distribution on a heterogeneous surface. In this model, $q_d$ reflects the adsorption capacity, while β is associated with the adsorption free energy (E)

based on the Eq. 15 [61]:

$$E\ (kJ/mol) = \frac{1}{\sqrt{2\beta}} \quad (15)$$

The value of E can be used to determine if adsorption is due to chemisorption (E > 8 kJ/mol), or physisorption (E < 8 kJ/mol) [62]. The values of E obtained in this study (0.224 kJ/mol for nZVI; 0.250 kJ/mol for SnZVI; and 0.071 kJ/mol for soil) indicated that As was immobilized on the surface of nanoparticles and soil via physisorption (Figure 8). Similar to the trend obtained from the Langmuir models, the trend of $q_d$, based on mass was nZVI (26.66 mg/g) > SnZVI (17.77 mg/g) >> soil (1.63 mg/g); but when compared using surface area normalized adsorption capacity, the trend was SnZVI (0.43 mg/$m^2$) > soil (0.31 mg/$m^2$) > nZVI (0.22 mg/$m^2$) The correlation coefficients obtained for three adsorbents ($R^2$ = 0.7018, 0.8730, 0.7178 for nZVI, SnZVI, and soil, respectively) were lower than other models. Thus, the D-R model is less capable of describing As adsorption in this study.

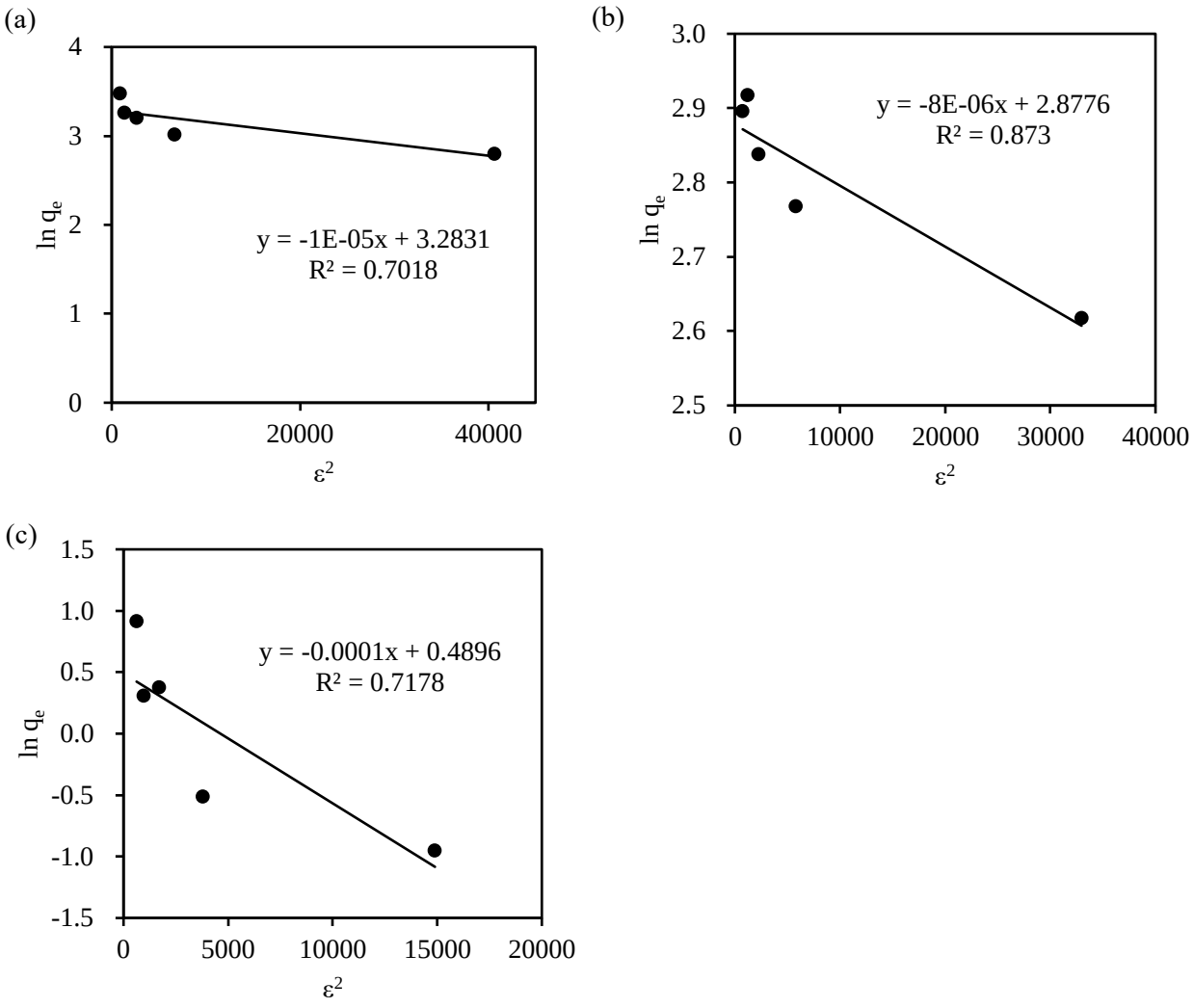


Figure 8. Modeling of adsorption of As to (a) nZVI, (b) SnZVI, and (c) soil (c) using the D-R isotherm

The parameters and correlation coefficients for each isotherm model are summarized in Table 3. This study shows that As could be adsorbed by nZVI, SnZVI, and soil in aqueous systems. However, only the adsorption of As by nZVI and SnZVI was favorable, based on Langmuir and Freundlich models. Based on the parameters obtained from the Langmuir and Temkin models, nZVI had a higher adsorption capacity than SnZVI on a mass basis. The capacity of soil for As was much lower than the capacity of both nanoparticles. Based on these findings, As could be immobilized by nZVI, SnZVI, and soil. However, nZVI

and SnZVI could outcompete soil for As adsorption in pore water, due to their much higher adsorption capacity and affinity. More so, nZVI may exhibit a better As immobilization efficiency than SnZVI in pore water if both nanoparticles are present at the same mass concentration.

Table 3. The correlation coefficient and parameters obtained from the adsorption isotherm models

| Models | Parameters | Adsorbents | | |
|---|---|---|---|---|
| | | nZVI | SnZVI | Soil |
| Langmuir | $R_2$ | 0.8881 | 0.9624 | 0.9427 |
| | $K_L$ | 0.089 | 0.186 | ND* |
| | $q_m$ (mg/g) | 31.25 | 19.16 | ND |
| | $q_N$ (mg/$m_2$) | 0.26 | 0.46 | ND |
| | $R_L$ | 0.26 | 0.22 | ND |
| Converted Langmuir | $R_2$ | 0.947 | 0.9977 | 0.1854 |
| | $K_L$ | 0.047 | 0.159 | ND |
| | $q_m$ (mg/g) | 37.31 | 19.53 | ND |
| | $q_N$ (mg/$m_2$) | 0.31 | 0.47 | ND |
| | $R_L$ | 0.36 | 0.24 | ND |
| Freundlich | $R_2$ | 0.9483 | 0.9669 | 0.9229 |
| | $K_F$ | 7.16 | 9.24 | 0.012 |
| | 1/n | 0.3221 | 0.1556 | 1.1314 |
| Temkin | $R_2$ | 0.8936 | 0.964 | 0.7937 |
| | $K_T$ (L/g) | 446 | 0.0009 | 93 |
| | b (J/mol) | 20291 | 6371 | 3638 |
| D-R | $R_2$ | 0.7018 | 0.873 | 0.7178 |
| | $q_d$ (mg/g) | 26.66 | 17.77 | 1.63 |
| | β (mol$_2$/J$_2$) | $1.00 \times 10^{-5}$ | $8.00 \times 10^{-6}$ | 0.0001 |
| | $q_N$ (mg/$m_2$) | 0.22 | 0.43 | 0.31 |
| | E (kJ/mol) | 0.224 | 0.250 | 0.071 |

*ND: not determinable

### 3.4. Soil remediation with nanoparticles

#### 3.4.1. Effect of nZVI sulfidation

As immobilization performance of nZVI and SnZVI in the soil was estimated by measuring the concentration of leachable As in soil 7 d after treatment with nanoparticles (Figure 9a). Compared with the untreated group, leachable As concentration decreased significantly in soils treated with 0.3%, 1%, and 5% nZVI ($p$ = 0.0004, 0.0002, and 0.0002, respectively) and SnZVI ($p$ = 0.0016, 0.0004, and 0.0002, respectively). As shown in Figure 9a, leachable As decreased to a larger extent when soil was treated with nZVI than when it was treated with SnZVI. Thus, sulfidation decreased the immobilization performance of nZVI, based on the 7 d remediation data. The immobilization efficiency was 93%, 98%, and 100% after 7 d when soil was treated with as 0.3%, 1%, and 5% nZVI, respectively. For SnZVI-treated soil, As immobilization efficiency after 7 d was 68%, 85%, and 100%, respectively. Although the immobilization efficiency of SnZVI was significantly lower than that of nZVI when the nanoparticles dosage applied for soil treatment were 0.3% and 1% ($p < 0.001$), the immobilization of As was similar for nZVI and SnZVI at 5% nanoparticle concentration. Thus, the first hypothesis of this study (that sulfidation improves the immobilization efficiency of nZVI for As) was rejected.

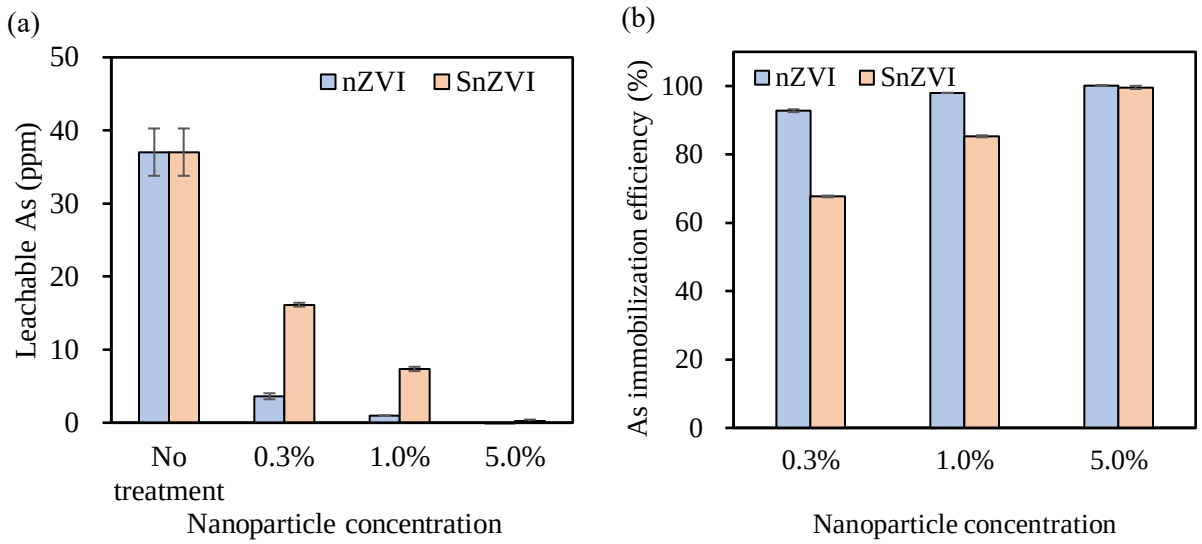


Figure 9. Remediation of soil contaminated with 50 ppm As by nZVI and SnZVI. (a) Leachable As concentration with and without nanoremediation after 7 d, (b) As immobilization efficiency at different nanoparticle dosage after 7 d.

To understand the mechanisms of As immobilization, the crystal structure of Fe, As, and S in treated and untreated contaminated soils were compared using XRD. In nZVI-treated soil (Figure 10a), the intensity of the peak at $2\theta = 36°$ and 46° decreased when As was present, suggesting that As impacted the $Fe_2O_3/Fe_3O_4$ shell of nZVI and co-precipitation of As with other oxides of iron may have occurred. In addition, new peaks were observed at $2\theta = 51°$, 56°, and 64° when As was present and were assigned to $As_4O_6$ and $As_2O_3$. The presence of these As species suggest that some of the As(V) spiked into the soil was reduced to As(III) by nZVI. Similarly, in the SnZVI group (Figure 10b), the increased signal at $2\theta = 32°$ implied that co-precipitation of As with oxides of Fe occurred. Moreover, reduced As ($As_4O_6$) was also observed in the SnZVI-treated soil, based on the new peaks at $2\theta = 42°$, 60°, and 66°. Differences in the diffractograms obtained in soils treated with nZVI and SnZVI suggest that sulfidation resulted in slightly different As

immobilization mechanism. For instance, a stronger peak at 2θ = 27° (assigned to $FeAsO_4$) was detected in the SnZVI-treated soil, demonstrating that the sulfidation promoted the formation of ferrous arsenate.

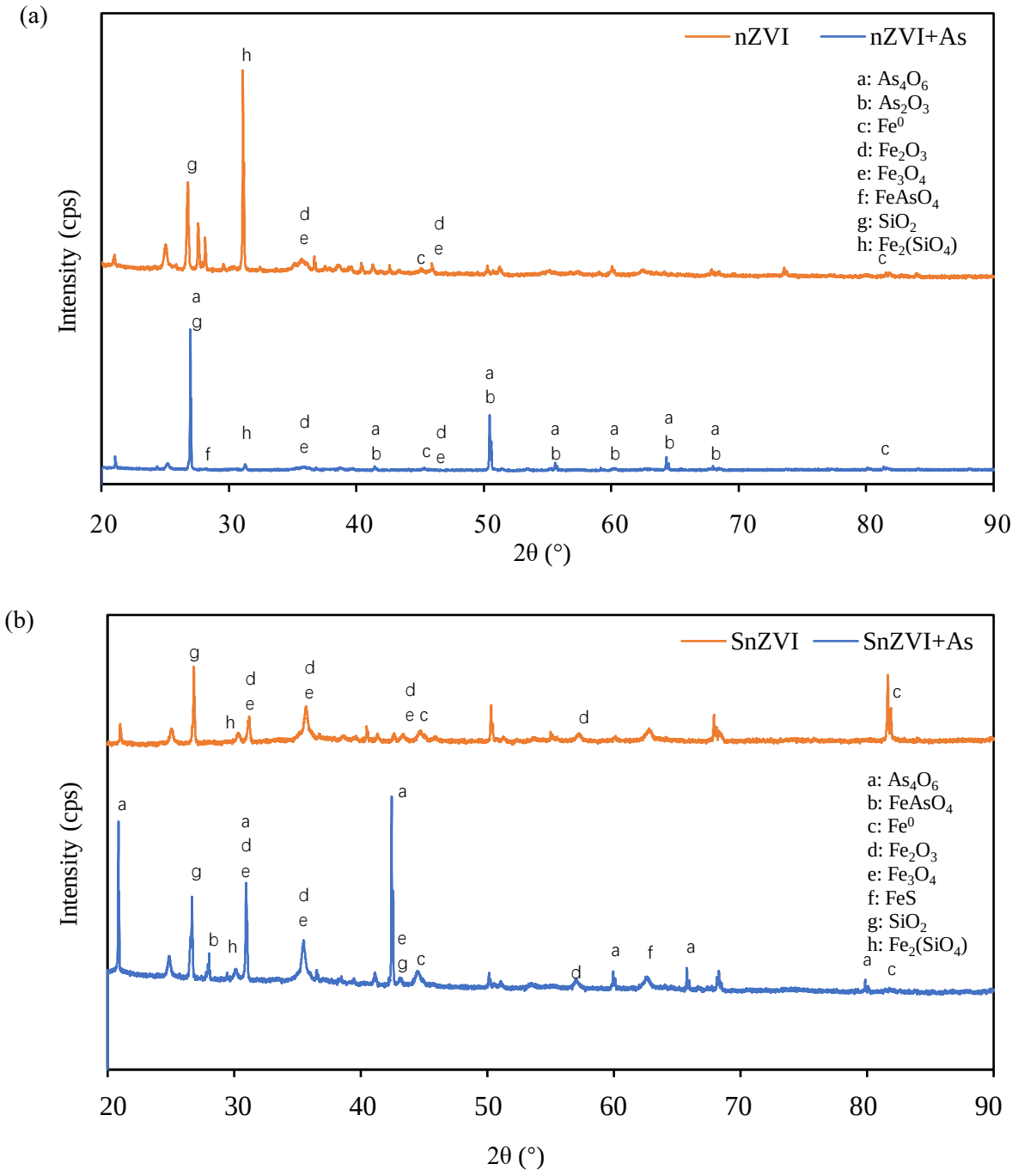


Figure 10. The XRD diffractograms of (a) nZVI- and (b) SnZVI-treated soil with and without As.

As shown in Figure 9a, only 37 ppm of As was leachable from untreated soil after 7 d, despite spiking it with 50 ppm of As. This confirms the adsorption studies that showed that the soil had some As immobilization capacity, howbeit, much lower than that of nZVI and SnZVI. Further investigation via XRD showed that components of soil could chemically bind to As. For instance, the peaks at 2θ = 43°, 60°, 67°, and 76° in Figure 11 were assigned to $AlAsO_4$, showing the binding of As to Al (e.g. from alumina). In addition, reduced As, in form of $As_4O_6$ at (2θ = 21°, 28°, and 35°), was found in untreated contaminated soil. As(V) may have been reduced by the reducing chemical agents in soil or by bacterial transformation.

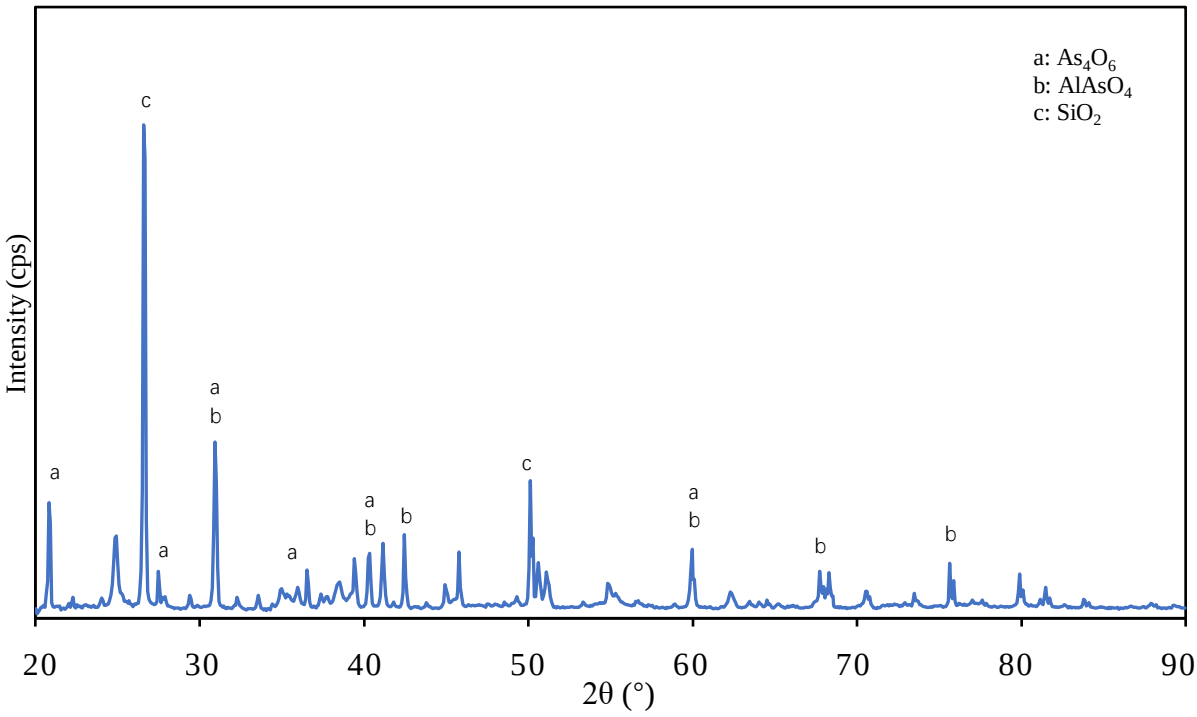


Figure 11. The XRD diffractograms of soil with As

Although no existing study has investigated the roles of sulfidation on nZVI's immobilization performance in soil, sulfidation was found to hinder the release of dissolved Fe from the nanoparticle in the aqueous

system [33]. The hinderance of nZVI dissolution also decreased the chances of co-precipitation (As-$Fe_2O_3$/$Fe_3O_4$), which is one of the mechanisms of As remediation by nZVI [63]. On the other hand, the sulfhydryl (-SH) group present in SnZVI increase the binding sites for heavy metals [33,64,65]. Therefore, the ratio of S/Fe of SnZVI likely plays an essential role in the As immobilization performance of SnZVI. A recent study showed that when the theoretical S/Fe ratio increased from 0 to 0.07, the Cd immobilization efficiency of SnZVI in water showed a downward trend; but as the ratio increased from 0.07 to 0.28, the immobilization efficiency for Cd improved and exceeded that of pristine nZVI when S/Fe ≥ 0.21 [33]. In future studies, the impact of S/Fe ratio on the immobilization of As in soil should be investigated.

### 3.4.2. Effect of treatment time

In the presence of oxygen and water, nZVI is transformed (Eq. 16 and 17), which may impact its long-term effectiveness. In fact, it has been reported that the active duration of nZVI towards contaminants in 4-8 weeks [66]. Thus, the effect of time on the As immobilization performance of both nanoparticles was investigated. In this study, the effectiveness of nZVI and SnZVI was monitored for 16 weeks by measuring leachable As concentration on days 7, 28, 56, and 112 As shown in Figure 12, the concentration of leachable As in the untreated soil continuously decreased over time, in agreement with findings from the adsorption and XRD studies that showed that the soil had a immobilization effects on As. However, after 28 d, there was no further significant decrease of leachable As over time in untreated soil ($p$ = 0.557 on day 56, and $p$ = 0.086 on day 112), indicating that As binding sites on soil was saturated by Day 28.

$$Fe^0 + 2H_2O \rightarrow Fe^{2+} + H_2 + 2OH^- \quad (16)$$

$$2Fe^0 + 4H^+ + O_2 \rightarrow 2Fe^{2+} + 2H_2O \quad (17)$$

In the 0.3% and 1% nZVI-treated soil, there was a significant increase in leachable As between days 7 and 28 ($p$ = 0.0007 and 0.0245, respectively), demonstrating remobilization of previously adsorbed As within this time period. The remobilization of As may be due to structural changes in nZVI due to aging, or the reduction of As(V) to As(III), which is more mobile in the environment (Figure 10a). Remobilization of As was not observed in the soil treated with 5% nZVI throughout the 16 weeks, indicating that high amounts of nZVI could be used to ensure immobilized As were not released later on. In contrast, the concentration of leachable As significantly decreased between days 7 and day 28 in contaminated soils treated with 0.3% ($p$ = 0.0001) and 1% ($p$ = 0.0025) SnZVI. The reasons may be due to the higher chemical stability of SnZVI and stronger binding due to the presence of -SH groups [33]. Like in nZVI-treated soils, As immobilization efficiency in soils treated with 5% SnZVI was 100% throughout the study. Although the As immobilization efficiency of nZVI was superior to that of SnZVI on Day 7 when both were used at 0.3 and 1%, the discrepancy in immobilization efficiency of both nanoparticles decreased over time: Differences in the leachable As concentration between soils treated with nZVI and SnZVI at 0.3 and 1% decreased from 12.6 and 6.4 ppm, respectively, on day 7 to 3.5 and 2.8 ppm, respectively, on day 112. In summary, SnZVI showed a slower immobilization kinetics compared to nZVI, but the remediation performances of both particles became more similar over time.

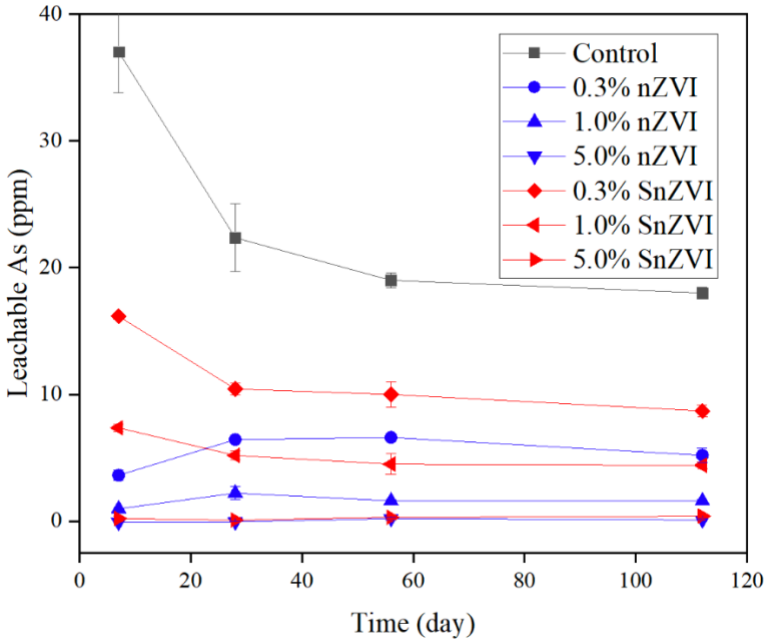


Figure 12. Leachable As concentration in soil over time change under aerobic conditions.

### 3.4.3. Effect of aeration

Since oxygen levels vary in soils, additional tests were performed to understand the impact of oxygen levels on As immobilization efficiencies of nZVI and SnZVI. Significantly lower immobilization efficiencies were observed in soils treated with 0.3 and 1% nZVI under aerobic conditions than soils treated with the same nanoparticle concentration under anoxic conditions except on day 7 ($p$ = 0.070 and 0.177 for 0.3% and 1%, respectively) (Figure 13). This finding indicates that anoxic conditions are more favorable for As immobilization by nZVI in soil. The advantage of anoxic conditions for As immobilization may be due to the impact of oxygen on the chemical stability of nZVI (Eq. 17) and transformation reduces the particles' binding sites [63]. Although slight increases in immobilization efficiency was observed when As-contaminated soils were treated with SnZVI under anoxic conditions, the difference in immobilization

efficiency between aerobic and anoxic conditions were only significant on day 112 ($p$ = 0.011 for 0.3%) and 0.014 for 1% SnZVI). The lower impact of oxygen levels on the immobilization of As by SnZVI is likely due to the improved chemical stability imparted by sulfidation. It should be noted that the As immobilization efficiency obtained when soils were treated with 5% nZVI and SnZVI was not sensitive to oxygen conditions (Figure 13).

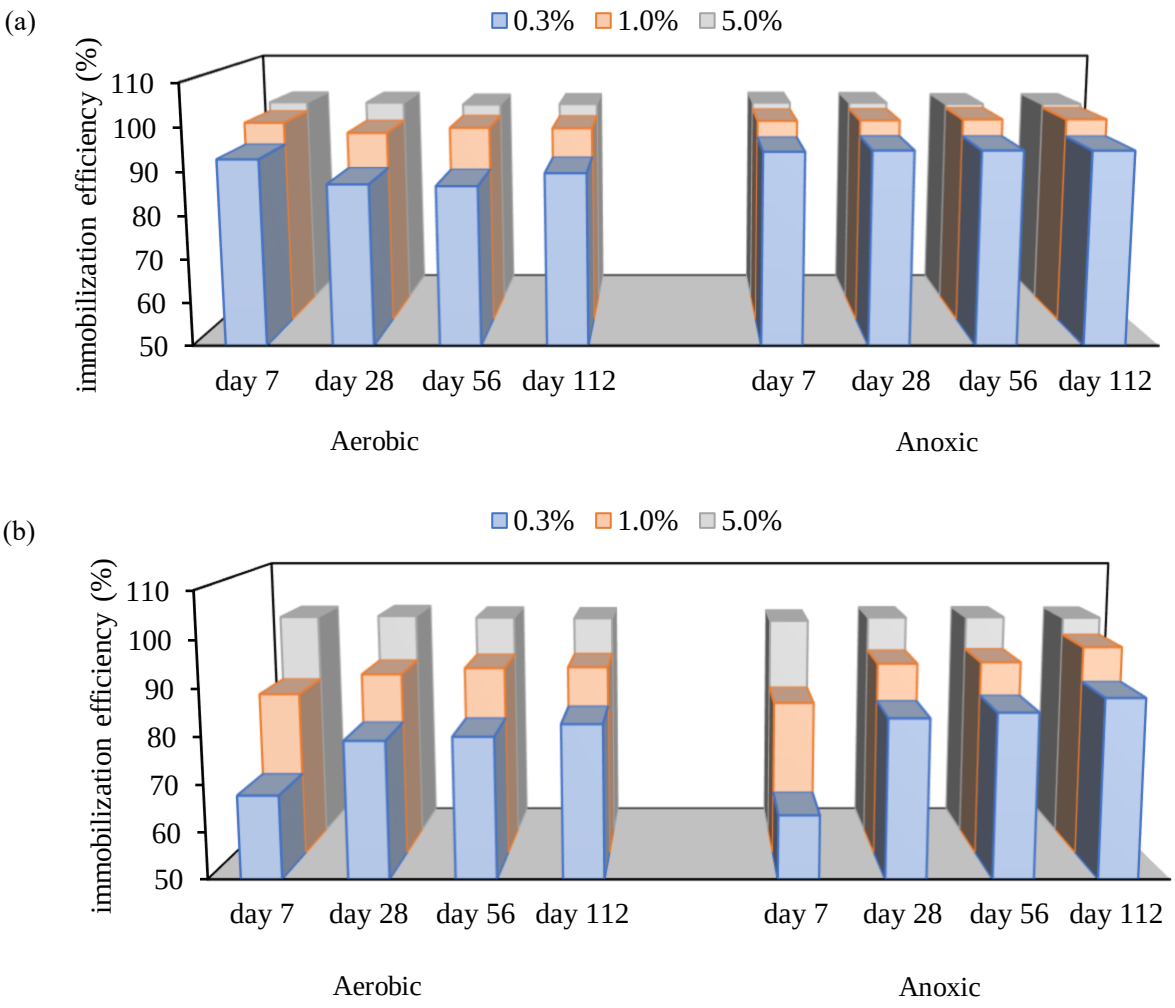


Figure 13. As immobilization efficiency of (a) nZVI, and (b) SnZVI in soil under aerobic and anoxic conditions for 112 days

### 3.4.4. Modeling of As immobilization with ANN

To predict the As immobilization efficiency of nZVI and SnZVI at different nanoparticle dosages, a new model was established using ANN. As shown in Figure 15, a new ANN function was accepted when the correlation coefficients between the target and output in training, validation, and test sections were higher than 0.95. Then, the immobilization efficiencies at different nanoparticle concentrations (51 equidistance points from 0% to 5%) were predicted using the new ANN function in MATLAB to obtain the plot shown in Figure 15a. The data was fitted with the model shown in Eq. 18 using Origin:

$$Immobilzation\ Efficiency\ (y) = y_0 - A \cdot e^{-\frac{c}{t}} \quad (18)$$

where $y_0$ (%) is the maximum efficiency; A (%) is the amplitude of efficiency (that is, maximum – minimum); c represents the nanoparticle concentration (%); and t is the concentration correction coefficient.

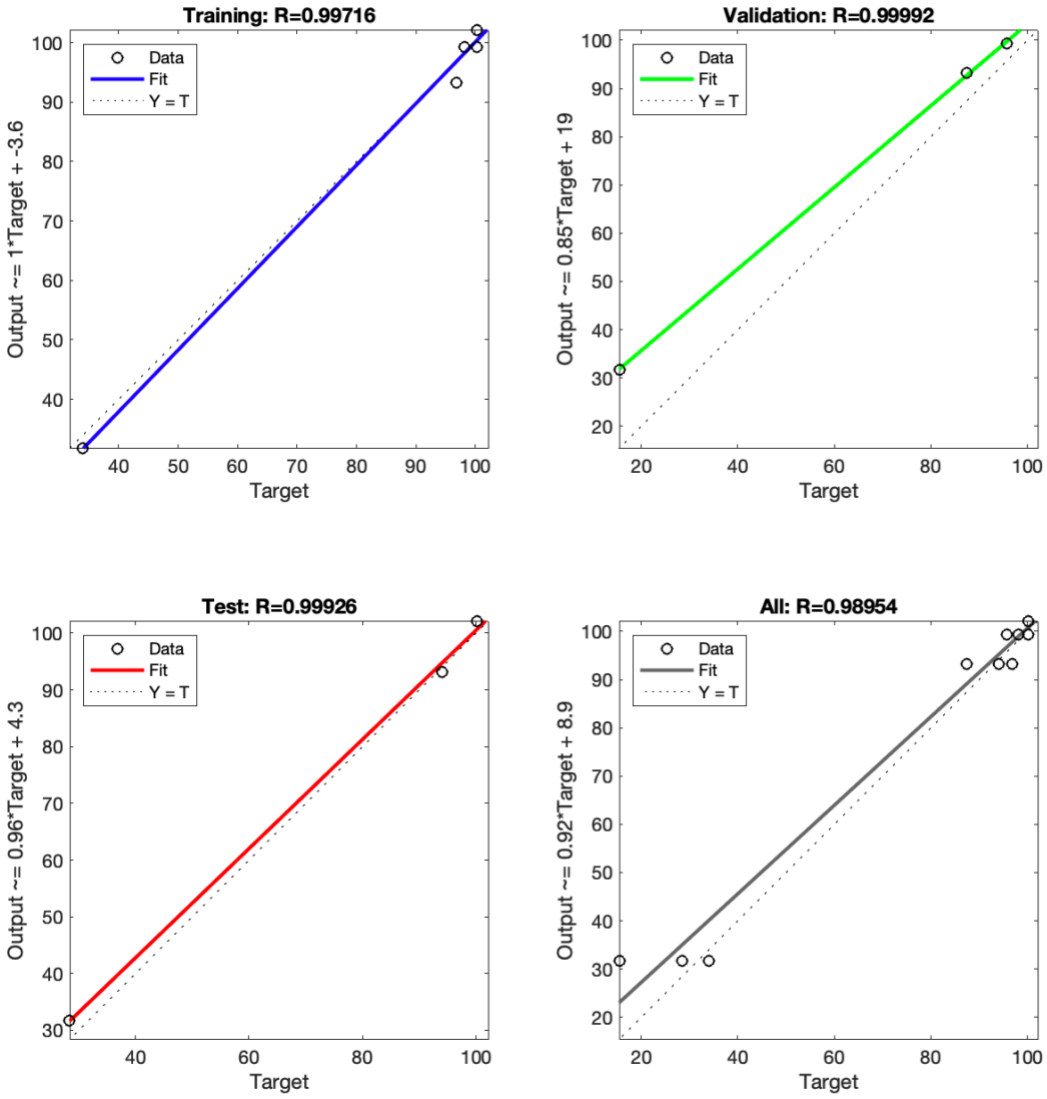


Figure 14. The correlation between the target value and output value in training, validation, and testing sections, as well as a combination of all three. The input data was the raw data of nZVI treatment group at 7 d.

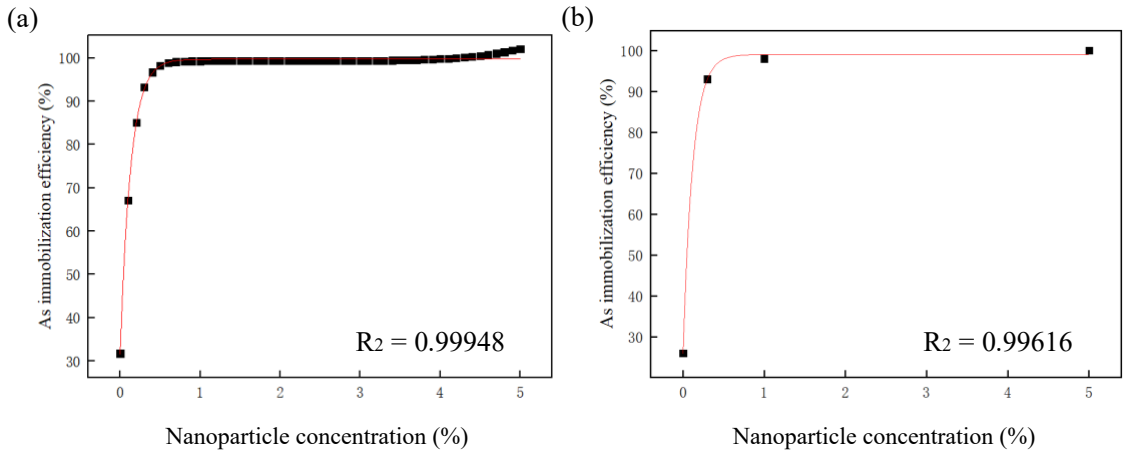


Figure 15. Fitting of mathematical function to (a) artificial neural network predicted data, and (b) the raw data obtained from experiments.

As shown in Figure 15 and Table 4, a high correlation coefficient ($R_2$ > 0.99) was obtained when the mathematical function in Eq. 16 was fitted with both ANN predicted data and the data obtained from experiments. Additionally, the parameters' values obtained from the predicted and raw dataset were very similar (relation deviation < 10%), demonstrating that ANN was successfully used to predict the immobilization of As by the nanoparticles, and Eq. 18 adequately describes the relationship between nanoparticle dosage and immobilization efficiency. Following this method, the immobilization efficiency obtained with different nanoparticles and times were also simulated ($R_2$ > 0.90) as shown in Figure 16. Therefore, machine learning has an excellent potential for predicting soil remediation efficiency with nZVI and SnZVI. In future studies, more parameters, such as treatment time, soil properties, or nanoparticle properties (S/Fe ratio, surface area, etc.), could be appropriately varied to further use machine learning to predict the results of remediation based on the other variables.

Table 4. Summary of the parameters obtained from fitting ANN and raw data (nZVI, day 7) to the function described in Eq. 18

| **nZVI (1 week)** | **$y_0$** | **A** | **t** | **$R_2$** |
|---|---|---|---|---|
| Prediction data (a) | 99 | 73 | 0.12 | 0.99948 |
| Raw data (b) | 100 | 68 | 0.13 | 0.99616 |
| Relative deviation | 1% | 7.4% | 7.7% | - |

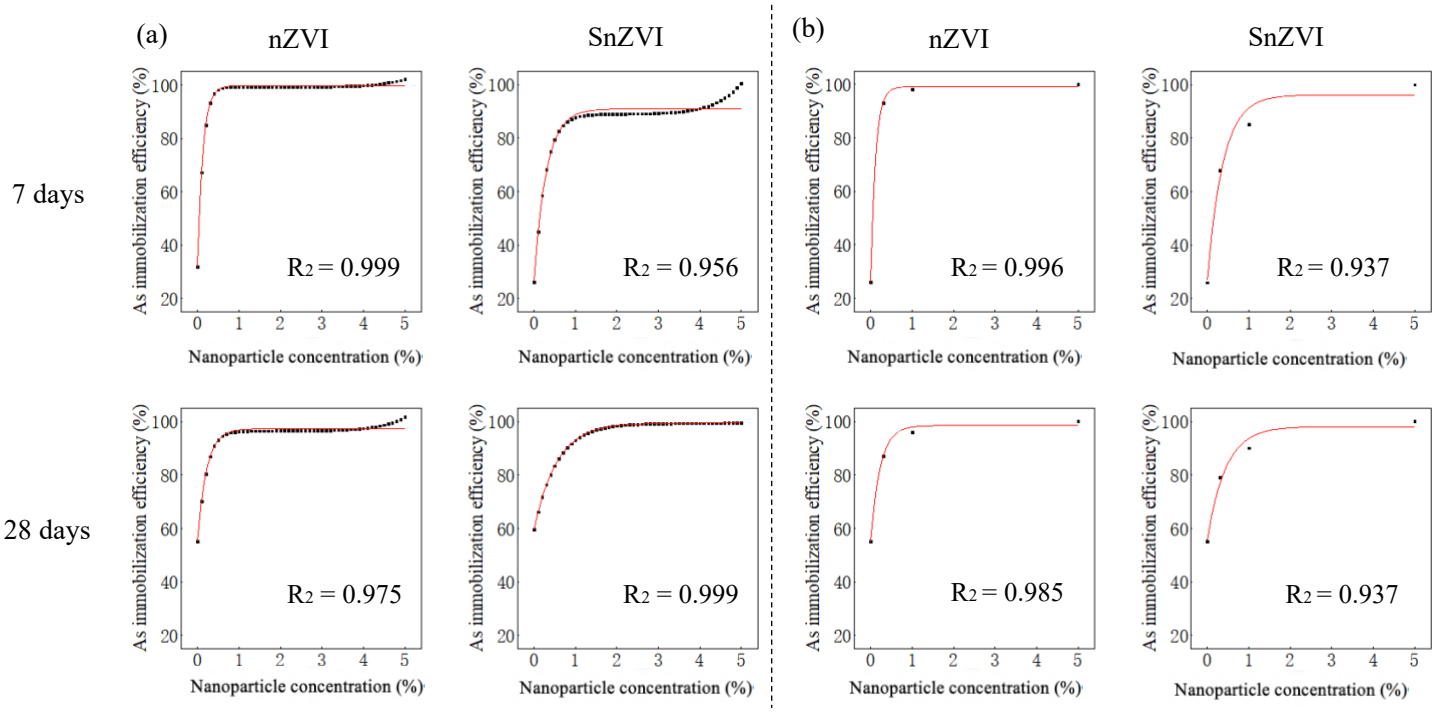


Figure 16. Fitting of mathematical function to (a) artificial neural network predicted data, and (b) the raw data obtained from experiments to all the data obtained on days 7 and 28

### 3.5. Environmental effects of remediation

#### 3.5.1. Effect on soil pH

The reactions of nZVI with water and dissolved oxygen generate hydroxide ions ($OH^-$) (Eq. 16 and 17), which increase soil pH. Increase in soil pH may affect speciation of chemical, surface properties of soil and particles, and the survival of sensitive organisms. Therefore, the effect of treating soil with nZVI and SnZVI on soil pH was evaluated. As shown in Figure 17, adding 0.3% of nanoparticles significantly increased the soil pH after 7 days ($p$ = 0.0000036 for nZVI and 0.0000316 for SnZVI). More impact was observed at higher nZVI concentrations. Sulfidation significantly negated change in soil pH at 0.3% ($p$ = 0.003), 1% ($p$ = 0.017) and 5% ($p$ = 0.011) treatment dosage. The lower impact of SnZVI on pH is likely due to the higher hydrophobicity of SnZVI and its lower reactivity with oxygen, both resulting in decreased tendency to undergo the reactions leading to the generation of $OH^-$. Additionally, the soil pH decreased after 28 days, which may be due to soil buffering effect, or the further hydrolysis of $Fe^{2+}$/$Fe^{3+}$ (Eq. 19 - 21), leading to reduction in soil pH.

$$Fe^{2+} + 2H_2O \rightarrow Fe(OH)_2 + 2H^+ \quad (19)$$

$$Fe^{3+} + 3H_2O \rightarrow Fe(OH)_3 + 3H^+ \quad (20)$$

$$H^+ + OH^- \rightarrow H_2O \quad (21)$$

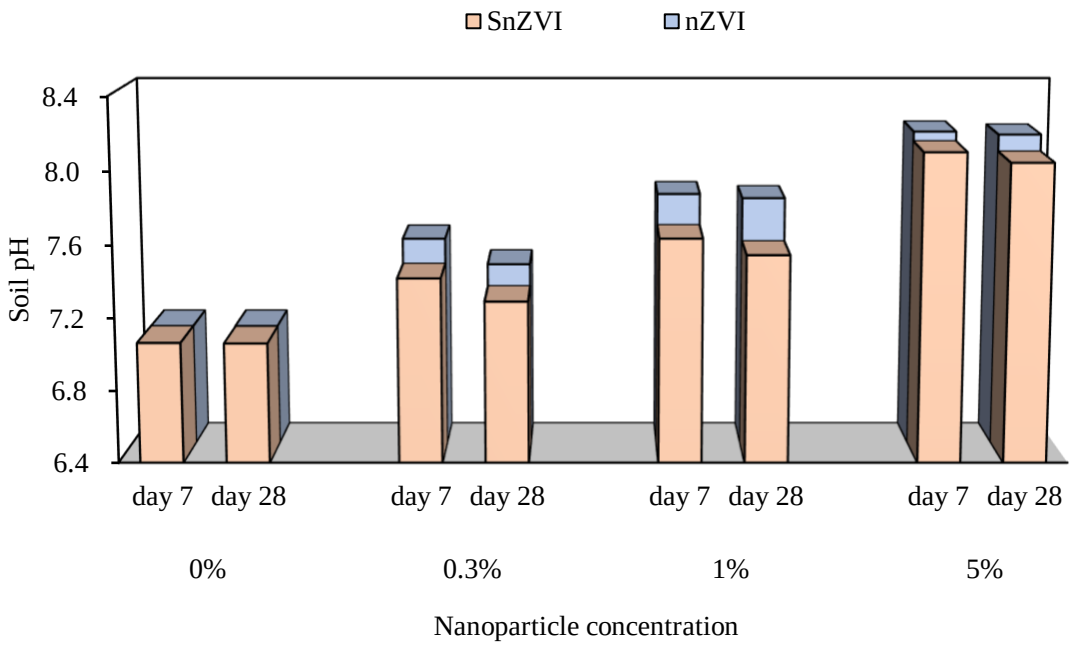


Figure 17. As-contaminated soil pH after 7 and 28 days, with and without treatment with nZVI and SnZVI

3.5.2. Effect on survival of *E. fetida*

After the two weeks of acute toxicity test, the mortality of adult earthworms in control group was below 10%, satisfying the requirement of the OECD 207 guideline. As shown in the data presented in Figure 18, the $LC_{50}$ for *E. fetida* was $145.1 \pm 17.8$ ppm. Based on this information, it was clear that most of the worms could survive at the selected test concentration for the As immobilization tests (50 ppm).

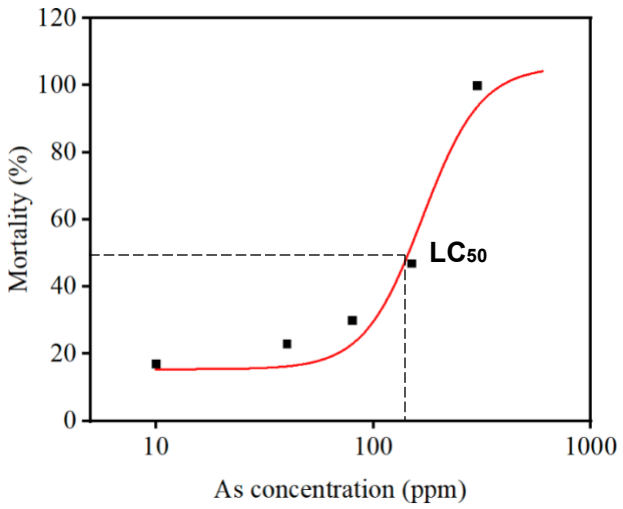


Figure 18. The mortality of *E. fetida* at different As concentration. The $LC_{50}$ was estimated as 145.1 $\pm$ 17.8 ppm.

The survival of *E. fetida* observed in the four-week toxicity study is shown in Figure 19. In the untreated soil, survival significantly decreased from 98% (in control group) to 60% after 28 d in the presence of 50 ppm As ($p$ = 0.0003). In general. the survival of *E. fetida* in As-contaminated soil decreased in the presence of nZVI. For instance, the addition of 1% nZVI caused all the earthworms to die within 7 d in the As-spiked soil (Figure 19a). Even at the lowest nZVI treatment concentration used in this study (0.3%), survival significantly decreased ($p$ = 0.000073) from 60% (untreated soil) to 10% after 28 d, indicating that soil remediation with nZVI caused additional toxicity to earthworms. However, sulfidation decreased the mortality of *E. fetida* caused by nZVI. At 0.3 and 1% SnZVI treatment dosage, survival *E. fetida* was 73% and 0% after 28 d. Additionally, there was no significant difference in *E. fetida* survival between untreated As-contaminated soil and soil treated with 0.3% SnZVI ($p$ = 0.177). Thus, the second hypothesis of this study (that sulfidation decreases the toxicity of nZVI) could not be rejected.

To confirm that the increased mortality of *E. fetida* in As-contaminated soil upon nanoremediation was mainly due to the nanoparticles, additional toxicity studies were performed with uncontaminated soil (As = 0 ppm) treated with the same concentrations of both nanoparticles. In general, the survival of *E. fetida* was similar to what we observed when contaminated soil was treated with the nanoparticles. As shown in Figure 19b, all the earthworms died within 28 d in the presence of 1% nZVI and SnZVI. At 0.3% nanoparticles concentration, survival decreased significantly relative to control groups ($p = 8.41 \times 10^{-10}$ for nZVI and $p = 0.0001$ for SnZVI). However, sulfidation reduced the toxicity of nZVI to earthworms, as reported earlier. The average survival of *E. fetida* exposed to 0.3% SnZVI (68%) after 28 d was significantly higher ($p = 0.00000219$) than those exposed to 0.3% nZVI (10%). In addition, the mortality rate was slower in the 1% SnZVI exposed group than the 1% nZVI group (where survival was 0% within 7 d). The toxicity of nZVI and SnZVI may originate from changes in soil properties (such as pH), increase in soil $Fe^{2+}/Fe^{3+}$ (due to dissolution and precipitation), and reactive oxygen species (ROS) generation by the nanoparticles [67,68]. Increased survival when soil was treated with SnZVI may be due to lower changes in soil pH (Figure16), less $Fe^{2+}/Fe^{3+}$ due to slower dissolution, and less ROS-induced oxidative stress due to higher chemical stability [41].

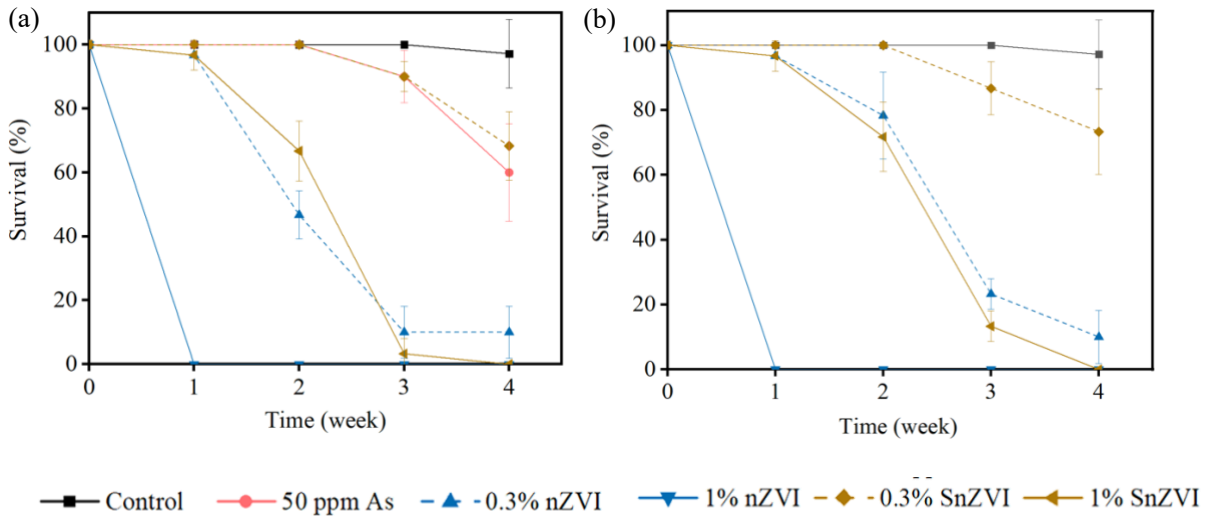


Figure 19. Average survival of *E. fetida* in the presence of 0, 0.3, and 1% nZVI and SnZVI in the (a) presence of 50 ppm, and (b) absence of As. The average survival of control group (no As and no nanoparticle) and nanoparticle control group (50 ppm As and no nanoparticle) were also shown for comparison.

In general, the average bodyweight of *E. fetida* in the nZVI-treatment and SnZVI-treatment groups (with or without As) decreased over 28 d, but significant difference in bodyweight was only found between the untreated group and SnZVI-treated group ($p$ = 0.00006 with As and $p$ = 0.002 without As). There was no significant difference between the change in weight of the control group and those kept in 50 ppm As-contaminated soil without treatment (p = 0.332), (2) those treated with 0.3% nZVI ($p$ = 0.413). Also, there was no significant difference in the weight of live earthworms exposed to 0.3% nZVI and SnZVI ($p$ = 0.074). The loss of biomass may be due to increased toxicity from As(III), which was produced in the presence of the nanoparticles (Figure 10), toxic effects of the nanoparticles themselves affecting earthworms growth and metabolism, or adsorption of nutrients to nanoparticles [69,68]. The specific reason

for decreased *E. fetida* biomass needs further studies.

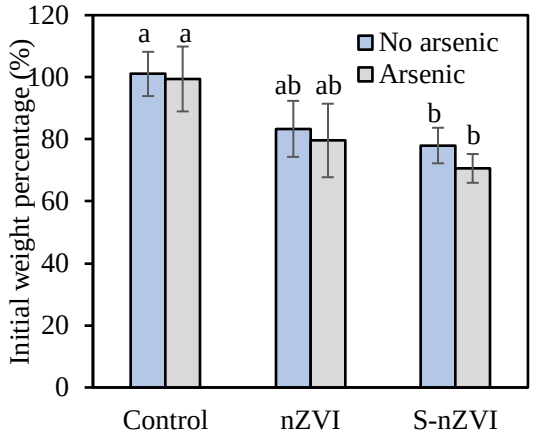


Figure 20. Change in *E. fetida* biomass in in soil treated with or without As and nanoparticles for 28 d. The initial weight percentage is the weight after 28 d divided by the initial weight. The concentration of As was 50 ppm, and the concentration of both nanoparticles was 0.3%. The control group was not treated with nanoparticles

### 3.5.3. Effect of pH on earthworm survival

During the 28 d toxicity test, a strong correlation ($R_2$ = 0.79) was observed between soil pH and *E. fetida* survival (Figure 21a). Thus, an additional toxicity test was set up to verify if increase in pH in the presence of the nanoparticles caused the increase in *E. fetida* mortality. Based on the results shown in Figure 21b, only 20% mortality was observed after 28 d when the soil pH was 8 soil. However, the mortality of *E. fetida* reached 90% and 100% after 28 d when soil was treated with 0.3% (pH = 7.41) and 1% (pH = 7.70) of nZVI, respectively (Figure 16), The wide discrepancy shows that while increased pH may decrease the survival of *E. fetida*, it is likely not the primary cause of mortality.

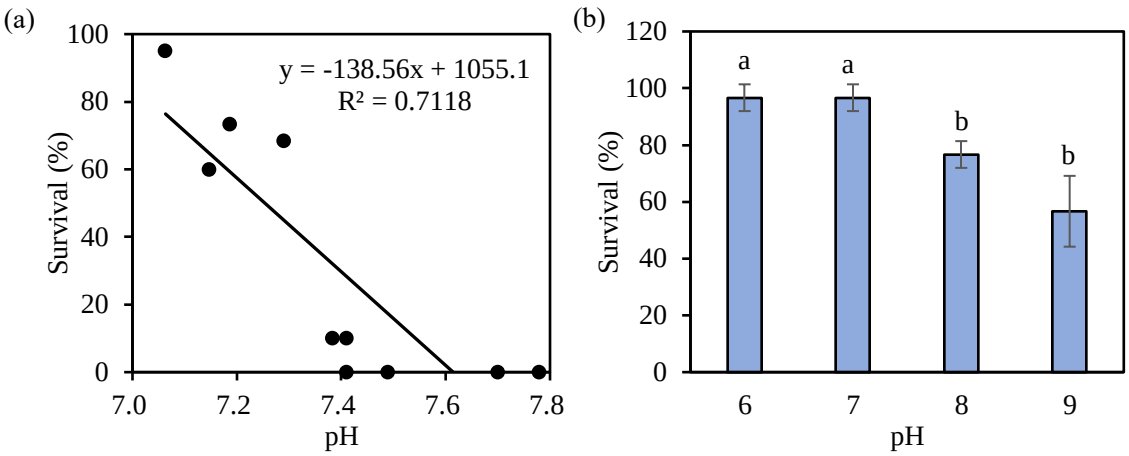


Figure 21. (a) Correlation between soil pH (in the presence of nanoparticles) and 28 d survival of *E. fetida*; (b) 28 d survival of *E. fetida* at different soil pH in the absence of nanoparticles.

### 3.6. As bioaccumulation by *E. fetida*

As has bioaccumulation and biomagnification effects, which is significant in that *E. fetida* serves as food source for higher organisms such as birds and moles [70]. As the results shown in (Figure 22), the average body burden of As in *E. fetida* kept in untreated As-spiked soil for 28 d was 1383 mg/kg (ppm) d.w., with BAF of 27.7 kg soil/kg earthworm. However, treatment of As-contaminated soil with 0.3% nZVI and SnZVI, significantly decreased the As concentration in *E. fetida* tissues to 130 ppm ($p$ = 0.010) and 266 ppm ($p$ = 0.012), respectively. The BAF decreased to 2.6 ($p$ = 0.012) and 5.3 ($p$ = 0.014), in the 0.3% nZVI- and SnZVI-treated groups, respectively. There was no significant difference in tissue As concentration in *E. fetida* grown in nZVI-treated soil and SnZVI-treated soil ($p$ = 0.364). These results reveal that although treatment of As-contaminated soil with nZVI and SnZVI may lead to lower survival of *E. fetida*, the nanoparticles decrease the bioavailability of As in soil, which is important for decreasing bioaccumulation of As up the food chain. Overall, SnZVI exhibited a much lower mortality to *E. fetida* compared to nZVI;

and yielded a statistically similar decrease in As bioaccumulation by the organism, making SnZVI a more sustainable option (than nZVI) for As immobilization.

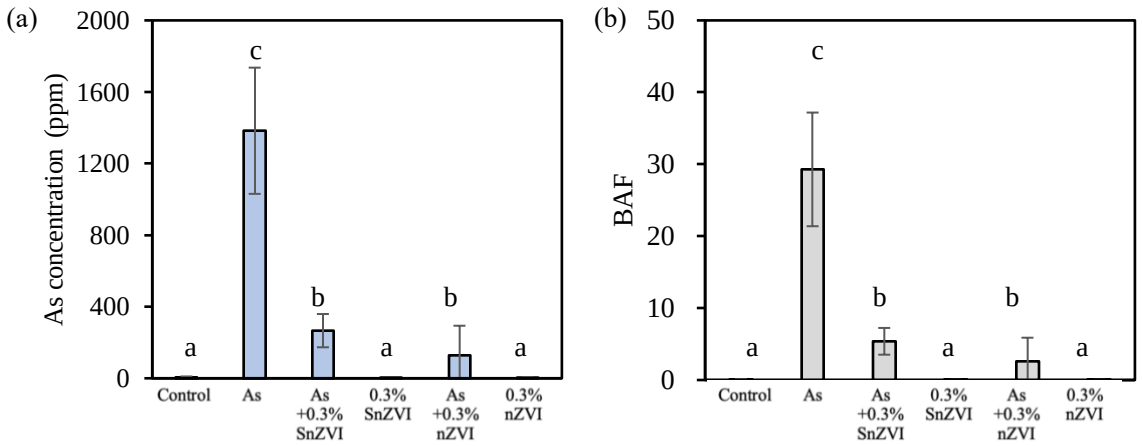


Figure 22 The As concentration (a) in earthworm bodies (dry weight) and BAF values (b)

## 4. Conclusions

The impact of sulfidation of nZVI on As immobilization performance in soil and its sustainability during remediation was evaluated in this study. Adsorption isotherm experiments conducted in aqueous media showed that nZVI and SnZVI can immobilized As via physisorption. On mass basis, sulfidation decreased the adsorption capacity for As from 31.25 mg/g (in nZVI) to 19.16 mg/g (in SnZVI). However, when the surface area per unit mass of each nanoparticle was considered, sulfidation actually improved the reactivity of nZVI, with As immobilization capacity increasing from 0.26 mg/$m_2$ to 0.46 mg/$m_2$. Soil immobilization efficiency studies revealed that 0.3% and 1% SnZVI has a lower immobilization efficiency for As than nZVI after 7 d. However, the immobilization efficiency of nZVI and SnZVI in soil became more similar over time, indicating that sulfidation decreased the reaction kinetic but not necessarily the adsorption capacity. Further comparison in aerobic and anoxic conditions demonstrated that high oxygen content led to nZVI corrosion and decreased immobilization performance. However, high oxygen content impacted the immobilization performance of SnZVI much less than that of nZVI. In addition to adsorption, XRD analysis provided proof for reduction of As(V) to As(III) by both nanoparticles, and co-precipitation of As with oxides of Fe.

Although both nZVI and SnZVI immobilized As in soil, the survival of *E. fetida* decreased in the presence of the nanoparticles at all treatment concentrations tested. However, sulfidation decreased the lethal effects of nZVI to *E. fetida*, providing an opportunity to further decrease the toxicity of nZVI by further tuning the S/Fe ratio. Treatment of As-contaminated soil with 0.3% SnZVI yielded a higher survival (73%) than with no treatment (60%) or treatment with nZVI (≤ 10%), demonstrating that treatment with SnZVI is a more

sustainable option nZVI. Although increase in pH partly explains the toxicity of the nanoparticles to *E. fetida*, higher pH was not the main cause of mortality. Other possible reasons for toxicity may be increased Fe concentration in soil, decreased availability of nutrients, and increased oxidative stress due to the activities of the nanoparticles.

This study shows that sulfidation can decrease the ecotoxicity of nZVI while not impacting its efficacy for soil remediation significantly. There is an opportunity to further change the S/Fe ratio of SnZVI to explore the potential for increased remediation performance while further decreasing its negative environmental effects. Future work should further probe the mechanism of nZVI and SnZVI immobilization of As in soil, particularly over a long time and under different soil conditions. In addition, the causes of the *E. fetida* death and weight change need further investigation.

# REFERENCES

(1) Lu, X.; Li, L. Y.; Wang, L.; Lei, K.; Huang, J.; Zhai, Y. Contamination Assessment of Mercury and Arsenic in Roadway Dust from Baoji, China. *Atmos. Environ.* **2009**, *43* (15), 2489–2496. https://doi.org/10.1016/j.atmosenv.2009.01.048.
(2) Nordstrom, D. K. PUBLIC HEALTH: Enhanced: Worldwide Occurrences of Arsenic in Ground Water. *Science* **2002**, *296* (5576), 2143–2145. https://doi.org/10.1126/science.1072375.
(3) Podgorski, J.; Berg, M. Global Threat of Arsenic in Groundwater. *Science* **2020**, *368* (6493), 845–850. https://doi.org/10.1126/science.aba1510.
(4) Huang, R.-Q.; Gao, S.-F.; Wang, W.-L.; Staunton, S.; Wang, G. Soil Arsenic Availability and the Transfer of Soil Arsenic to Crops in Suburban Areas in Fujian Province, Southeast China. *Sci. Total Environ.* **2006**, *368* (2–3), 531–541. https://doi.org/10.1016/j.scitotenv.2006.03.013.
(5) Baba, A.; Sözbilir, H. Source of Arsenic Based on Geological and Hydrogeochemical Properties of Geothermal Systems in Western Turkey. *Chem. Geol.* **2012**, *334*, 364–377. https://doi.org/10.1016/j.chemgeo.2012.06.006.
(6) Costello, R. J.; Eller, P. M.; Hull, R. D. Measurement of Multiple Inorganic Arsenic Species. *Am. Ind. Hyg. Assoc. J.* **1983**, *44* (1), 21–28. https://doi.org/10.1080/15298668391404301.
(7) Mikutta, C.; Mandaliev, P. N.; Mahler, N.; Kotsev, T.; Kretzschmar, R. Bioaccessibility of Arsenic in Mining-Impacted Circumneutral River Floodplain Soils. *Environ. Sci. Technol.* **2014**, *48* (22), 13468–13477. https://doi.org/10.1021/es502635t.
(8) Sloth, J. J.; Julshamn, K.; Lundebye, A.-K. Total Arsenic and Inorganic Arsenic Content in Norwegian Fish Feed Products. *Aquac. Nutr.* **2005**, *11* (1), 61–66. https://doi.org/10.1111/j.1365-2095.2004.00334.x.
(9) Peryea, F. J.; Creger, T. L. Vertical Distribution of Lead and Arsenic in Soils Contaminated with Lead Arsenate Pesticide Residues. *Water. Air. Soil Pollut.* **1994**, *78* (3–4), 297–306. https://doi.org/10.1007/BF00483038.
(10) Whitmore, T. J.; Riedinger-Whitmore, M. A.; Smoak, J. M.; Kolasa, K. V.; Goddard, E. A.; Bindler, R. Arsenic Contamination of Lake Sediments in Florida: Evidence of Herbicide Mobility from Watershed Soils. *J. Paleolimnol.* **2008**, *40* (3), 869–884. https://doi.org/10.1007/s10933-008-9204-8.
(11) *Scientific Investigations Report*; Scientific Investigations Report; Scientific Investigations Report; 2019.
(12) Thomas, K. W.; Pellizzari, E. D.; Berry, M. R. Population-Based Dietary Intakes and Tap Water Concentrations for Selected Elements in the EPA Region V National Human Exposure Assessment Survey (NHEXAS). *J. Expo. Sci. Environ. Epidemiol.* **1999**, *9* (5), 402–413. https://doi.org/10.1038/sj.jea.7500051.
(13) Tripathi, R. M.; Raghunath, R.; Krishnamoorthy, T. M. Arsenic Intake by the Adult Population in Bombay City. *Sci. Total Environ.* **1997**, *208* (1–2), 89–95. https://doi.org/10.1016/S0048-9697(97)00278-7.
(14) Waring, J.; Maher, W. Arsenic Bioaccumulation and Species in Marine Polychaeta.

*Appl. Organomet. Chem.* **2005**, *19* (8), 917–929. https://doi.org/10.1002/aoc.938.
(15) Barwick, M.; Maher, W. Biotransference and Biomagnification of Selenium Copper, Cadmium, Zinc, Arsenic and Lead in a Temperate Seagrass Ecosystem from Lake Macquarie Estuary, NSW, Australia. *Mar. Environ. Res.* **2003**, *56* (4), 471–502. https://doi.org/10.1016/S0141-1136(03)00028-X.
(16) Ratnaike, R. N. Acute and Chronic Arsenic Toxicity. *Postgrad. Med. J.* **2003**, *79* (933), 391–396. https://doi.org/10.1136/pmj.79.933.391.
(17) Priority List of Hazardous Substances; ATSDR - Agency for Toxic Substances and Disease Registry, 2019.
(18) Teaf, C. M.; Covert, D. J.; Teaf, P. A.; Page, E.; Starks, M. J. Arsenic Cleanup Criteria for Soils in the US and Abroad: Comparing Guidelines and Understanding Inconsistencies. *Water Energy* **2010**, *15* (1), 10.
(19) Chen, J.; Sun, G.-X.; Wang, X.-X.; Lorenzo, V. de; Rosen, B. P.; Zhu, Y.-G. Volatilization of Arsenic from Polluted Soil by *Pseudomonas Putida* Engineered for Expression of the *ArsM* Arsenic(III) S-Adenosine Methyltransferase Gene. *Environ. Sci. Technol.* **2014**, *48* (17), 10337–10344. https://doi.org/10.1021/es502230b.
(20) Singhakant, C.; Koottatep, T.; Satayavivad, J. Enhanced Arsenic Removals through Plant Interactions in Subsurface-Flow Constructed Wetlands. *J. Environ. Sci. Health Part A* **2009**, *44* (2), 163–169. https://doi.org/10.1080/10934520802539780.
(21) Jang, M.; Hwang, J. S.; Choi, S. I.; Park, J. K. Remediation of Arsenic-Contaminated Soils and Washing Effluents. *Chemosphere* **2005**, *60* (3), 344–354. https://doi.org/10.1016/j.chemosphere.2004.12.018.
(22) Miretzky, P.; Cirelli, A. F. Remediation of Arsenic-Contaminated Soils by Iron Amendments: A Review. *Crit. Rev. Environ. Sci. Technol.* **2010**, *40* (2), 93–115. https://doi.org/10.1080/10643380802202059.
(23) Beesley, L.; Marmiroli, M. The Immobilisation and Retention of Soluble Arsenic, Cadmium and Zinc by Biochar. *Environ. Pollut.* **2011**, *159* (2), 474–480. https://doi.org/10.1016/j.envpol.2010.10.016.
(24) Qiao, J.; Liu, T.; Wang, X.; Li, F.; Lv, Y.; Cui, J.; Zeng, X.; Yuan, Y.; Liu, C. Simultaneous Alleviation of Cadmium and Arsenic Accumulation in Rice by Applying Zero-Valent Iron and Biochar to Contaminated Paddy Soils. *Chemosphere* **2018**, *195*, 260–271. https://doi.org/10.1016/j.chemosphere.2017.12.081.
(25) Hartley, W.; Lepp, N. W. Remediation of Arsenic Contaminated Soils by Iron-Oxide Application, Evaluated in Terms of Plant Productivity, Arsenic and Phytotoxic Metal Uptake. *Sci. Total Environ.* **2008**, *390* (1), 35–44. https://doi.org/10.1016/j.scitotenv.2007.09.021.
(26) Karn, B.; Kuiken, T.; Otto, M. Nanotechnology and *in Situ* Remediation: A Review of the Benefits and Potential Risks. *Environ. Health Perspect.* **2009**, *117* (12), 1813–1831. https://doi.org/10.1289/ehp.0900793.
(27) Adeleye, A. S.; Conway, J. R.; Garner, K.; Huang, Y.; Su, Y.; Keller, A. A. Engineered Nanomaterials for Water Treatment and Remediation: Costs, Benefits, and Applicability. *Chem. Eng. J.* **2016**, *286*, 640–662. https://doi.org/10.1016/j.cej.2015.10.105.

(28) Su, C.; Puls, R. W.; Krug, T. A.; Watling, M. T.; O'Hara, S. K.; Quinn, J. W.; Ruiz, N. E. A Two and Half-Year-Performance Evaluation of a Field Test on Treatment of Source Zone Tetrachloroethene and Its Chlorinated Daughter Products Using Emulsified Zero Valent Iron Nanoparticles. *Water Res.* **2012**, *46* (16), 5071–5084. https://doi.org/10.1016/j.watres.2012.06.051.
(29) Mueller, N. C.; Braun, J.; Bruns, J.; Černík, M.; Rissing, P.; Rickerby, D.; Nowack, B. Application of Nanoscale Zero Valent Iron (NZVI) for Groundwater Remediation in Europe. *Environ. Sci. Pollut. Res.* **2012**, *19* (2), 550–558. https://doi.org/10.1007/s11356-011-0576-3.
(30) O'Carroll, D.; Sleep, B.; Krol, M.; Boparai, H.; Kocur, C. Nanoscale Zero Valent Iron and Bimetallic Particles for Contaminated Site Remediation. *Adv. Water Resour.* **2013**, *51*, 104–122. https://doi.org/10.1016/j.advwatres.2012.02.005.
(31) Adeleye, A. S.; Stevenson, L. M.; Su, Y.; Nisbet, R. M.; Zhang, Y.; Keller, A. A. Influence of Phytoplankton on Fate and Effects of Modified Zerovalent Iron Nanoparticles. *Environ. Sci. Technol.* **2016**, *50* (11), 5597–5605. https://doi.org/10.1021/acs.est.5b06251.
(32) Li, S.; Wang, W.; Liang, F.; Zhang, W. Heavy Metal Removal Using Nanoscale Zero-Valent Iron (NZVI): Theory and Application. *J. Hazard. Mater.* **2017**, *322*, 163–171. https://doi.org/10.1016/j.jhazmat.2016.01.032.
(33) Su, Y.; Adeleye, A. S.; Keller, A. A.; Huang, Y.; Dai, C.; Zhou, X.; Zhang, Y. Magnetic Sulfide-Modified Nanoscale Zerovalent Iron (S-NZVI) for Dissolved Metal Ion Removal. *Water Res.* **2015**, *74*, 47–57. https://doi.org/10.1016/j.watres.2015.02.004.
(34) Lv, D.; Zhou, X.; Zhou, J.; Liu, Y.; Li, Y.; Yang, K.; Lou, Z.; Baig, S. A.; Wu, D.; Xu, X. Design and Characterization of Sulfide-Modified Nanoscale Zerovalent Iron for Cadmium(II) Removal from Aqueous Solutions. *Appl. Surf. Sci.* **2018**, *442*, 114–123. https://doi.org/10.1016/j.apsusc.2018.02.085.
(35) Stevenson, L. M.; Adeleye, A. S.; Su, Y.; Zhang, Y.; Keller, A. A.; Nisbet, R. M. Remediation of Cadmium Toxicity by Sulfidized Nano-Iron: The Importance of Organic Material. *ACS Nano* **2017**, *11* (10), 10558–10567. https://doi.org/10.1021/acsnano.7b05970.
(36) Lv, D.; Zhou, J.; Cao, Z.; Xu, J.; Liu, Y.; Li, Y.; Yang, K.; Lou, Z.; Lou, L.; Xu, X. Mechanism and Influence Factors of Chromium(VI) Removal by Sulfide-Modified Nanoscale Zerovalent Iron. *Chemosphere* **2019**, *224*, 306–315. https://doi.org/10.1016/j.chemosphere.2019.02.109.
(37) Fajardo, C.; Gil-Díaz, M.; Costa, G.; Alonso, J.; Guerrero, A. M.; Nande, M.; Lobo, M. C.; Martín, M. Residual Impact of Aged NZVI on Heavy Metal-Polluted Soils. *Sci. Total Environ.* **2015**, *535*, 79–84. https://doi.org/10.1016/j.scitotenv.2015.03.067.
(38) Pongratz, R. Arsenic Speciation in Environmental Samples of Contaminated Soil. *Sci. Total Environ.* **1998**, *224* (1–3), 133–141. https://doi.org/10.1016/S0048-9697(98)00321-0.
(39) Calderon, B.; Fullana, A. Heavy Metal Release Due to Aging Effect during Zero Valent Iron Nanoparticles Remediation. *Water Res.* **2015**, *83*, 1–9. https://doi.org/10.1016/j.watres.2015.06.004.
(40) Keller, A. A.; Garner, K.; Miller, R. J.; Lenihan, H. S. Toxicity of Nano-Zero Valent Iron to Freshwater and Marine Organisms. *PLoS ONE* **2012**, *7* (8), e43983.

https://doi.org/10.1371/journal.pone.0043983.
(41) Kim, E.-J.; Le Thanh, T.; Kim, J.-H.; Chang, Y.-S. Synthesis of Metal Sulfide-Coated Iron Nanoparticles with Enhanced Surface Reactivity and Biocompatibility. *RSC Adv.* **2013**, *3* (16), 5338. https://doi.org/10.1039/c3ra00009e.
(42) Adeleye, A. S.; Keller, A. A.; Miller, R. J.; Lenihan, H. S. Persistence of Commercial Nanoscaled Zero-Valent Iron (NZVI) and by-Products. *J. Nanoparticle Res.* **2013**, *15* (1), 1418. https://doi.org/10.1007/s11051-013-1418-7.
(43) Yiming, S.; Jassby, D.; Zhang, Y.; Keller, A. A.; Adeleye, A. S. Comparison of the Colloidal Stability, Mobility, and Performance of Nanoscale Zerovalent Iron and Sulfidated Derivatives. *J. Hazard. Mater.* **2020**, 122691. https://doi.org/10.1016/j.jhazmat.2020.122691.
(44) Kim, E.-J.; Kim, J.-H.; Azad, A.-M.; Chang, Y.-S. Facile Synthesis and Characterization of Fe/FeS Nanoparticles for Environmental Applications. *ACS Appl. Mater. Interfaces* **2011**, *3* (5), 1457–1462. https://doi.org/10.1021/am200016v.
(45) Carbonell-Barrachina, A. A.; Jugsujinda, A.; Burlo, F.; Delaune, R. D.; Patrick, W. H. Arsenic Chemistry in Municipal Sewage Sludge as Affected by Redox Potential and PH. *Water Res.* **2000**, *34* (1), 216–224. https://doi.org/10.1016/S0043-1354(99)00127-X.
(46) Bissen, M.; Frimmel, F. H. Arsenic — a Review. Part I: Occurrence, Toxicity, Speciation, Mobility. *Acta Hydrochim. Hydrobiol.* **2003**, *31* (1), 9–18. https://doi.org/10.1002/aheh.200390025.
(47) Xu, J.; Wang, Y.; Weng, C.; Bai, W.; Jiao, Y.; Kaegi, R.; Lowry, G. V. Reactivity, Selectivity, and Long-Term Performance of Sulfidized Nanoscale Zerovalent Iron with Different Properties. *Environ. Sci. Technol.* **2019**, *53* (10), 5936–5945. https://doi.org/10.1021/acs.est.9b00511.
(48) Adeleye, A. S.; Ho, K. T.; Zhang, M.; Li, Y.; Burgess, R. M. Fate and Transformation of Graphene Oxide in Estuarine and Marine Waters. *Environ. Sci. Technol.* **2019**, *53* (10), 5858–5867. https://doi.org/10.1021/acs.est.8b06485.
(49) OECD. *Guideline for Testing of Chemicals 207, Earthworm, Acute Toxicity Tests*; 2007.
(50) Nelson, D. W.; Sommers, L. E. Total Carbon, Organic Carbon, and Organic Matter. In *Agronomy Monographs*; Page, A. L., Ed.; American Society of Agronomy, Soil Science Society of America: Madison, WI, USA, 2015; pp 539–579. https://doi.org/10.2134/agronmonogr9.2.2ed.c29.
(51) Chen, M.; Ma, L. Q.; Harris, W. G. Arsenic Concentrations in Florida Surface Soils: Influence of Soil Type and Properties. *Soil Sci. Soc. Am. J.* **2002**, *66* (2), 632–640. https://doi.org/10.2136/sssaj2002.6320.
(52) Galdames, A.; Mendoza, A.; Orueta, M.; de Soto García, I. S.; Sánchez, M.; Virto, I.; Vilas, J. L. Development of New Remediation Technologies for Contaminated Soils Based on the Application of Zero-Valent Iron Nanoparticles and Bioremediation with Compost. *Resour.-Effic. Technol.* **2017**, *3* (2), 166–176. https://doi.org/10.1016/j.reffit.2017.03.008.
(53) Gil-Díaz, M.; Alonso, J.; Rodríguez-Valdés, E.; Pinilla, P.; Lobo, M. C. Reducing the Mobility of Arsenic in Brownfield Soil Using Stabilised Zero-Valent Iron Nanoparticles. *J. Environ. Sci. Health Part A* **2014**, *49* (12), 1361–1369.

https://doi.org/10.1080/10934529.2014.928248.
(54) Azari, P.; Bostani, A. A. Reducing As Availability in Calcareous Soils Using Nanoscale Zero Valent Iron. *Environ. Sci. Pollut. Res.* **2017**, *24* (25), 20438–20445. https://doi.org/10.1007/s11356-017-9447-x.
(55) Liesch, A. M. Impact of Two Different Biochars on Earthworm Growth and Survival. *Ann. Environ. Sci.* **2010**, *v. 4*, 1–0.
(56) ISO (International Organization for Standardization). *Soil Quality - Determination of PH*, No. 10390.; ISO: Geneve, 2005.
(57) Kamitani, T.; Kaneko, N. Species-Specific Heavy Metal Accumulation Patterns of Earthworms on a Floodplain in Japan. *Ecotoxicol. Environ. Saf.* **2007**, *66* (1), 82–91. https://doi.org/10.1016/j.ecoenv.2005.10.009.
(58) Everett, D. H. Basic Principles of Colloid Science. In *RSC Paperbacks*; Royal Society of Chemistry: Cambridge, 2007; pp P001–P004. https://doi.org/10.1039/9781847550200-FP001.
(59) Dada, A. O.; Olalekan, A. P.; Olatunya, A. M.; DADA, O. Langmuir, Freundlich, Temkin and Dubinin–Radushkevich Isotherms Studies of Equilibrium Sorption of Zn 2+ Unto Phosphoric Acid Modified Rice Husk. *J. Appl. Chem.* **2012**, *3* (1), 38–45.
(60) Ghogomu, J. Removal of Pb(II) Ions from Aqueous Solutions by Kaolinite and Metakaolinite Materials. *Br. J. Appl. Sci. Technol.* **2013**, *3* (4), 942–961. https://doi.org/10.9734/BJAST/2013/4384.
(61) Ayawei, N.; Ebelegi, A. N.; Wankasi, D. Modelling and Interpretation of Adsorption Isotherms. *J. Chem.* **2017**, *2017*, 1–11. https://doi.org/10.1155/2017/3039817.
(62) S, M. S.; M, E. A. A.; Chidambaram, R. Isotherm Modelling, Kinetic Study and Optimization of Batch Parameters Using Response Surface Methodology for Effective Removal of Cr(VI) Using Fungal Biomass. *PLOS ONE* **2015**, *10* (3), e0116884. https://doi.org/10.1371/journal.pone.0116884.
(63) Zhang, Y.; Su, Y.; Zhou, X.; Dai, C.; Keller, A. A. A New Insight on the Core–Shell Structure of Zerovalent Iron Nanoparticles and Its Application for Pb(II) Sequestration. *J. Hazard. Mater.* **2013**, *263*, 685–693. https://doi.org/10.1016/j.jhazmat.2013.10.031.
(64) Wu, D.; Peng, S.; Yan, K.; Shao, B.; Feng, Y.; Zhang, Y. Enhanced As(III) Sequestration Using Sulfide-Modified Nano-Scale Zero-Valent Iron with a Characteristic Core–Shell Structure: Sulfidation and As Distribution. *ACS Sustain. Chem. Eng.* **2018**, *6* (3), 3039–3048. https://doi.org/10.1021/acssuschemeng.7b02787.
(65) Mullet, M.; Boursiquot, S.; Abdelmoula, M.; Génin, J.-M.; Ehrhardt, J.-J. Surface Chemistry and Structural Properties of Mackinawite Prepared by Reaction of Sulfide Ions with Metallic Iron. *Geochim. Cosmochim. Acta* **2002**, *66* (5), 829–836. https://doi.org/10.1016/S0016-7037(01)00805-5.
(66) Zhang, W. Nanoscale Iron Particles for Environmental Remediation: An Overview. *J. Nanoparticle Res.* **2003**, *5* (3/4), 323–332. https://doi.org/10.1023/A:1025520116015.
(67) Cheng, Y.; Dong, H.; Lu, Y.; Hou, K.; Wang, Y.; Ning, Q.; Li, L.; Wang, B.; Zhang, L.; Zeng, G. Toxicity of Sulfide-Modified Nanoscale Zero-Valent Iron to Escherichia Coli in Aqueous Solutions. *Chemosphere* **2019**, *220*, 523–530.

https://doi.org/10.1016/j.chemosphere.2018.12.159.
(68) Liang, J.; Xia, X.; Zhang, W.; Zaman, W. Q.; Lin, K.; Hu, S.; Lin, Z. The Biochemical and Toxicological Responses of Earthworm (Eisenia Fetida) Following Exposure to Nanoscale Zerovalent Iron in a Soil System. *Environ. Sci. Pollut. Res.* **2017**, *24* (3), 2507–2514. https://doi.org/10.1007/s11356-016-8001-6.
(69) Martínez-Fernández, D.; Komárek, M. Comparative Effects of Nanoscale Zero-Valent Iron (NZVI) and Fe 2 O 3 Nanoparticles on Root Hydraulic Conductivity of Solanum Lycopersicum L. *Environ. Exp. Bot.* **2016**, *131*, 128–136. https://doi.org/10.1016/j.envexpbot.2016.07.010.
(70) Ma, T.; Chen, L.; Wu, L.; Zhang, H.; Luo, Y. Oxidative Stress, Cytotoxicity and Genotoxicity in Earthworm Eisenia Fetida at Different Di-n-Butyl Phthalate Exposure Levels. *PLOS ONE* **2016**, *11* (3), e0151128. https://doi.org/10.1371/journal.pone.0151128.